MICROELECTRONIC BIOINSTRUMENTATION
SYSTEMS - NGR-36-027-053

Proposal and Progress Report
June 15, 1976
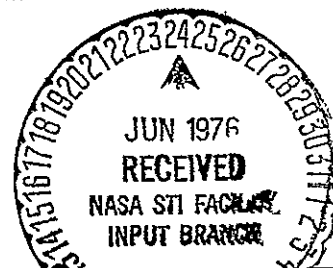
MICROELECTRONIC BIOINSTRUMENTATION SYSTEMS

NGR-36-027-053

Submitted to

AMES RESEARCH CENTER

NATIONAL AERONAUTICS and SPACE ADMINISTRATION

Wen H. Ko, Ph.D
Principal Investigator
Director-
Engineering Design Center

Research Administration

ENGINEERING DESIGN CENTER

Case Institute of Technology
Case Western Reserve University

Cleveland, Ohio 44106

ERRATA

Page	Location	Correction
6	Paragraph 2, line 1	NGR 36-027-053
A-4	Paragraph 2, line 7	tests
A-44	Last line	latex
A-46		Latex
A-51	Paragraph 2, line 2	the
A-52	Paragraph 2, line 2	If the requirement...

TABLE OF CONTENTS

NASA BUDGET PROPOSAL

SEPT 30, 1976 to SEPT 30, 1977

PERSONNEL				COST/SHARING
Ko	1100	5%	$2,043.	$1,247.
Sun	1190	25%	4,500.	
Kou	1200	10 mos.	6,000.	
Homa	1600	20%	2,704.	
Greene	1600	23%	3,273.	
	Personnel Costs		$18,520.	$1,247.
	Fringe 15.5%		2,870.	193.
	Total Salary		$21,390.	$1,440.
SUPPLIES	3100		4,000.	
TRAVEL	3400		1,000.	
PUBLICATION & COMMUNICATION	3500		1,000.	
TOTAL DIRECT COSTS			$27,390.	$1,440.
46% OVERHEAD			12,610.	660.
TOTAL BUDGET			$40,000.	$2,100.

PERSONNEL CHANGES

Dr. Jarsolav Hynecek left in February of 1976. Mr. John Homa replaced him and will carry out the single channel telemetry system work.

Dr. Sun will join this department in August of 1976. He will work 25% on the project with Dr. Ko.

BIOGRAPHICAL SKETCH

(Give the following information for all professional personnel listed on page 3, beginning with the Principal Investigator.
Use continuation pages and follow the same general format for each person.)

NAME	TITLE	BIRTHDATE *(Mo., Day, Yr.)*
SUN, Rai - Ko	Visiting Scientist, Engineering Design Center	December 11, 1922

PLACE OF BIRTH *(City, State, Country)*	PRESENT NATIONALITY *(If non-U.S. citizen, indicate kind of visa and expiration date)*	SEX
Kwangtung, China		[X] Male [ ] Female

EDUCATION *(Begin with baccalaureate training and include postdoctoral)*

INSTITUTION AND LOCATION	DEGREE	YEAR CONFERRED	SCIENTIFIC FIELD
Swiss Federal Institute of Technology, Zurich, Switzerland	D. Sc.	1955	Electrical Engineerir
University of London, King's College, London, England, Great Britain	M. Sc.	1953	Electrical Engineeri
National Chekiang University, Hanchow	B.S.E.E.	1946	Electrical Engineerir

HONORS

Senior Member - I. E. E. E.

MAJOR RESEARCH INTEREST	ROLE IN PROPOSED PROJECT
Biomedical Instrumentation, Electrosurgery and Electrotherapy	Visiting Scientist

RESEARCH SUPPORT *(See instructions)*

RESEARCH AND/OR PROFESSIONAL EXPERIENCE *(Starting with present position, list training and experience relevant to area of project. List a or most representative publications. Do not exceed 3 pages for each individual.)*

PROFESSIONAL EXPERIENCE:

1964-Present	Research Scientist, Siemens Company, Erlangen, West Germany
1961-1964	Research Fellowship, University of Stuttgart, Stuttgart, Germany
1958-1961	Research and Development Engineer, Landis and Gyr Company, Zug, Switzerlan
1954-1958	Research Fellow, Swiss Federal Institute of Technology, Zurich, Switzerlan
1950-1954	Postgraduate Student, University of London, King's College, London, England, Great Britain
1949-1950	Power Engineer, British Thomson-Houston Company, Rugby, England, Great Britain
1946-1949	Assistant Professor, Department of Electrical Engineering, National Chekiang University, Shanghai, China
	Design Engineer, Wha-Tung Electrical Manufacturing Company, Shanghai, Chin

PUBLICATIONS:

1. "Stray Load Losses Due to the Radial Component of Leakage Flux in a Core Type Power Transformer." British Electrical and Allied Industries Research Association, ERA, London, England, (1952).

2. "Leistungsmessung und Leistungsregulierung in Mehphasen-netzen mittels Halbleitern", with Strutt, M. J. O. Archiv f. Elektrotechnik, Vol. 42, Heft 3, pp. 155-164, (1955).

3. "Experimentelle und theoretische Untersuchung von Halbleiter-Halleffektoszillatoren" with Strutt, M. J. O. Archiv d. Elektrischen Uebertragung, Vol. 11, No. 6,

pp. 261-265, (1957).

4. "Mehrphasenwattmeter beruhend auf der magnetischen Widerstandsanderung von Halbleitern", with Strutt, M. J. O. Bulletin des Schweizerchen Elektrotechnischen Vereins, No. 10, p. 308, (1959).

5. "Multiphase Wattmeter Based on the Magnetoresistance Effect of Semiconductors", Strutt, M. J. O. IRE Transactions on Instrumentation, Vol. I-10, No. 1, pp. 44-49, (1961).

6. "Oscillators by Means of Magnetoresistance Effect." Proceedings IRE, Vol. 50, No. 6, pp. 1484-1493, (June, 1962).

7. "Determination of the Thermal Time Constant of InSb Hall Element." Proceedings IEEE, Vol. 51, No. 9, p. 1255, (September, 1963).

8. "Magnetoresistance of InSb at a Microwave Frequency." Journal of Applied Physics, Vol. 35, No. 1, pp. 211-214, (January, 1964).

9. "Application of Magnetoresistance of InSb to Mixer in Microwave Range." Solid State Electronics, Vol. 7, pp. 373-377, (1964).

10. "Theory and Applications of a Three Dimensional Multiplier by Means of Magnetoresistance." Solid State Electronics, Vol. 7, pp. 363-371, (1964).

11. "Magnetoresistance Better than Hall Effect Multiplier." Electronics, U. S. A., pp. 66-70, (April 6, 1964).

12. "Leistungsmessung in Mikrowellenbereich mittels Gauss Effekt von InSb-NiSb." Archiv d. Elektrischen Uebertragung, Vol. 18, No. 11, pp. 662-664, (1964).

13. "Magnetoresistance of InSb-NiSb at Microwave Frequency." Solid State Electronics, Vol. 8, pp. 344-346, (1965).

14. "Investigation on a Magnetoresistance Element with A. C. Bias and its Application to Electronic Devices." Archiv d. Elektrischen Uebertrgung, Vol. 19, No. 10, pp. 565-570, (1965).

15. "Application of a Gauss Effect Element to Magnetic Recording." IEEE Transactions on Audio, Vol. AU 13, No. 2, (1965).

16. "Die Widerstandsanderung von InSb in hohen Magnetfeldern overhalb Zimmertemperatur", with Wagini, H. Zeitschrift f. angewandte Physik, Vol. 20, No. 5, pp. 318-322, (1966).

17. "Improvement of Superconducting Nb Cavities by Anodic Oxide Films", with Martens, H. and Dipers, H. Physics Letters, Vol. 34A, No. 7, pp. 439-440, (1971).

18. "Electron Paramegnetic Resonance Study on Mixed Crystals $Ce_{1-x}Gd_xRu_2$", with Schnitzke, K. Physics Letters, Vol. 35A, No. 4, pp. 263-264, (1971).

19. "A New Method of Electropolishing Niobium", with Dipers, H, Schmidt, O., and Martens, H. Physics Letters, Vol. 37A, No. 2, pp. 139-140, (1971).

20. "Experimente mit elektromechanischen Antrieben fur ein kuenstliches Herz", with Haerten, R. and Geisselbrecht, G. Fachberichteder Jahrestagung der Deutschen

Gesellschaft fur Biomedizinische Technik, p. 141, Erlangen, West Germany, (May, 1973).

21. "Experiments on Electromechanical Driving Systems for Aritficial Heart", with Haerten, R. and Geisselbrecht, G. Digest of the Tenth International Conference on Medical and Biological Engineering, p. 136, Dresden, DDR, Germany, (August 13-17, 1973).

22. "Ein incorporierbares Antriebssystem fur Blutpumpen zur Entlastung des linken Herzens", with Geisselbrecht, G., Haerten, R., Karpil, L. and Seifert, A. Biomedizinische Technik, Vol. 19, No. 6, pp. 217-224, (December, 1974).

23. "Experimente mit einem inkorporierbaren Antriebssystem fur Blutpumpen zur Entlastung des linken Herzens", with Geisselbrecht, G.; Haerten, R., Karpil, L., Seifert, A. and Gresse, H. Biomedizinische Technik, Vol. 20, No. 1, pp. 15-21, (February, 1975).

5

MICROELECTRONICS BIOINSTRUMENTATION SYSTEMS PROPOSAL

For the 1975 to 1976 year (from October 1, 1975 to September 30, 1976) up to the present date, we have made progress in the single channel ECG telemetry system, RF cage design, and three channel ECG, pressure, and temperature telemetry system. The progress reports for these projects are given in Appendix A.

For the continuation of Research Grant NGR-36-027-053, for the 1976 to 1977 year (10/1/76-9/30/77), we propose to perform the following work in accordance with the budget on page 1.

1. RF Powered Single Channel ECG Telemetry System

The work needed to be performed in this area includes modification of the existing circuit to obtain a wider margin of operation such that alignment changes between the implant and the external coil will allow proper system operation. This on going project will also include the fabrication of three new devices to replace the old device implanted in the monkey.

2. RF Powered Animal Cage Single Channel ECG Telemetry System

Two units for implantation in a monkey which is kept alive in a cage with the dimensions 40"x20"x20", will be constructed. The animal will be free moving within the cage and three detector coils will be used to receive the RF power at various orientations. The necessary task for this project includes:

a) Provide ventilation of the cage and at the same time maintain low leakage of the RF field.

b) Assemble three detector coils for powering of the single channel system.

c) Glass encapsulate and design an assembly procedure to produce the detector.

d) Animal evaluation to be performed at this institution with rabbits.

e) Provide the system to NASA for evaluation in monkeys.

3. <u>RF Cage Three Channel ECG, Pressure, and Temperature Telemetry System</u>

This project will be a continuation of the development of the three channel bench model designed and constructed in the 1975-1976 period. Tasks to be carried out include:

a) Development of the present design to hybrid form.

b) Development of a packaging scheme to enable the pressure transducer to operate in the blood stream.

c) Design of a three coil detector to power the telemetry system.

d) Glass encapsulation of the unit.

e) Animal evaluation to be done at this institution with rabbits.

f) Evaluation of the system at NASA with monkeys.

ANNUAL REPORT

RESEARCH GRANT   NGR 36-027-053

MICROELECTRONIC BIOINSTRUMENTATION SYSTEMS

July 1975 to June 1976

Submitted to

NATIONAL AERONAUTICS and SPACE ADMINISTRATION

Dr. Wen H. Ko

Case Institute of Technology
CASE WESTERN RESERVE UNIVERSITY

Cleveland, Ohio   44106

APPENDIX A

PROGRESS REPORTS

Objectives

To determine suitable encapsulation materials for chronic implantation of electronic circuits in the body. These materials must only increase the volume of the implant minimally, be nearly impervious to water, be an electrical insulator when chronically implanted, have good mechanical strength and adherence. Also, they must not require temperatures over 60°C in their application for circuits with batteries and over 200°C for other circuits, and be compatible with biologic tissue.

Report

The materials testing has been primarily aimed at finding a packaging method for a pressure transducer; a case which presents the most difficult requirements. Ideally the material must protect the device both electrically and mechanically without effecting sensitivity or stability. For a pressure transducer application the package must be able to insulate the welded wire attachments on the sensors; it is calculated that the resistance seen between the attachments must be at least 125 megohms for less than 1mm shift in the output. The optimum package, for the purpose of sealing, is one in which the sensor and the wire attachments are completely coated. Such a package has no coating to transducer interfaces open to body fluids to act as leakage paths. The requirements for such a coating are that it be elastic enough to cover the sensing diaphragm without reducing the sensitivity of the device. It is of course desirable that the coating adhere to the transducer surface and, because it will be bearing directly on the diaphragm, the coating should have a coefficient of thermal expansion close to that of silicon. Alternately, a coating with a high elasticity and compliance allows a greater mismatch in thermal coefficients.

A materials testing procedure has been used in which a standard electrode is coated with the material under study and subjected to leakage resistance tests. The test electrode consists of a ceramic substrate upon which two separate thick film gold contacts have been fired. These contacts are in turn connected to lead wires by soldering, and epoxy is coated over the solder joints for adherence and protection. The entire structure is sketched in Figure D-1. This substrate is coated with various encapsulation materials by a multiple dipping and drying process as determined by the requirements of the material. After drying or curing, the encapsulation substrate is immersed in its own test tube of physiologic saline maintained at 40°C in an oil bath. The leads exiting from the tube are regularly connected to a testing circuit which measures resistance up to 200 gigaohms.

The first studies on packaging materials centered on the use of epoxies. The epoxy materials have, however, proved less than successful in the same applications particularly those involving transducers. Originally it was thought that only the wire attachment area would need to be coated; giving the advantage of having the sensing diaphragm unobstructed. This type of package has the drawback of having several interfaces which can cause leakage. The excellent adhesion of epoxy and silicon, thermal stresses were created in the transducer, causing drift and hysteresis. Where a soft compliant coating would have minimized these factors the adherence and rigidity of epoxy were actually detrimental. Also, because of their ionic nature, the epoxies had severly reduced insulation resistance in fluid enviroments. The epoxy materials were therefore rejected as packaging components.

Of the other materials studied, the most promising have been the polymers; Kraton; and Epcar, Polyurethane, Silicone Rubber RTV; Parylene and Silicon Filled Epoxy. The data collected on these materials is summarized in the data tables that follow. Besides these materials; tests have been done on wax, varnish, nitrile rubber, plastisol, acrylic cement, silastic and Q dope. None of these materials was suitable and data on them is not included in this report.

The polymer materials, Kraton, and Epcar gave good results in the electrode tests. Kraton in particular gave excellent results, and most of the studies were made on this material. Kraton formed thin layers when dip coated and was soft and flexible; suggesting that it would make a suitable coating. There are, however, several problems with Kraton. The coating solution was very difficult to prepare and it was not possible to prepare a solution of the same concentration consistently. The solution would dry very quickly and skin over making repeated coating difficult. Since the solution was normally 90% solvent (cyclohexane) the material showed excessive shrinkage as it dried. The shrinkage and low viscosity of the solution combined to give poor coatings especially around the edges and corners. The Kraton materials also had very poor adhesion, particularly to silicon dioxide. Adhesion varied widely and was on the order of 200 grams per square centimeter and was increased to approximately 500 grams/cm^2 if briefly heated over 150°C. It was not determined if this was due to melting of the Kraton or chemical decomposition.

The Epcar material showed much poorer insulation properties than the Kraton and also poorer adhesion unless heated. When heated to approximately 160°C (melting point) the Epcar adhesion increased to the order of 500 grams per square centimeter. The Epcar solution was much thicker than the Kraton solution but showed similar problems of shrinkage and coverage.

Polyurethane gave widely varied results depending on how it was prepared and applied. Extreme care had to be taken during application to get a uniform bubble free coating.

The most recent tests show that a coating of 25 mils on test electrodes would last for 15 days. The adhesion of the polyurethane compounds showed strengths on the order of 2 kg per square centimeter on silicon dioxide, however the peel strength was considerably lower than this figure. The polyurethane compounds may be mixed to give various degrees of hardness, with all the mixtures producing a relatively tough coating. In tests on diaphragms the polyurethane greatly increased hysteresis and temperature effects. Hysteresis was on the order of 100 mmHg for a 30°C temperature cycle and temperature coefficients increased one order of magnitude. Overall, the polyurethane has good mechanical strength, fair adhesion, and fair insulation properties, combined with severe temperature and sensitivity results.

Parylene coatings have excellent mechanical strength, being very hard and stiff. Parylene shows very poor adhesion to silicon, although no quantitative measurements have been made. As an insulating layer, results have been inconsistent. The first parylene tests had a thickness of 125 mils and seemed to be of poor quality. For this test 5 diaphragms were examined, none which lasted more than 5 days. The second run had a coating thickness of 4 mils and was of good quality. The testing of this run is not complete; however indications are that this material will not be superior to others already tested. The temperature and sensitivity effects of parylene are very bad. Testing 3 sensors, sensitivity has been reduced 60 to 90 per cent, temperature coefficients have been raised by at least one order of magnitude and hysteresis is at least 200 mmHg over 30°C.

It was hoped that by mixing finely divided silicon into an epoxy mixture that the thermal expansion of epoxy could be matched to that caused by epoxy. It was also hoped that the silicon filler would increase the insulation resistance of the coating, by lengthening the conduction paths. The improvements obtained were insufficient to overcome the reduced insulating ability of epoxy due to ionic migration in fluids. The packages failed unexpectedly and completely after about two weeks, and no temperature tests were made on this material.

Several tests were done on polyethylene coatings. By dissolving polyethylene in a heated solvent thin coatings with excellent adhesion were produced. However, insulation test results were inconsistent. It is believed that pin-holes are left in the coating by the evaporating solvent. It was necessary to use a very high percentage of solvent in coating preparation to produce a workable solution, also the solution must be heated during repeated dipped coatings.

The silicone rubber materials have given the most consistant results in the insulation testing, several sensors and diaphragms have lasted over a month in saline solution. The adhesion of the silicone rubber to silicon dioxide is exceptional,

although their adherence to metal is only fair. The limiting factor is adhesion for this material is its low mechanical strength; however the material is quite soft and flexible and transmits pressure well. The silicone rubbers cause less than 1% reduction in pressure sensitivity and because of its extreme elasticity temperature effects are minimal. Tests to this date show hysteresis effects typically less than 1mm for a 30°C cycle.

The first silicone rubber tests were made using commercial grade coatings for electronics packaging. Extensive tests were done on Dow Corning 3140; because of the success of these tests, further trials were made on medical grade materials. Excellent results have been found with Medical Type A adhesive. Tests are also being done on MDX 4210; this material has less adhesion than type A but has superior mechanical properties. At the present time characterization of the coating properties of these materials are being made, this includes saline immersion tes and temperature cycling. These materials are currently being tried in several applications.

The final material under consideration is teflon. This material has excellent insulation properties, but is difficult to process and cannot be fluidized for coating as other materials are tested. At this time attempts are being made to coat teflon using rf sputtering. Some work on this technique has been done by NASA at the Lewis Research Center.

In addition to the materials tests, work is being done to improve the physical aspects of the coating process. To this end sensors are being trimmed with a high speed dental drill to remove sharp corners and small globes of solder which formed along the sides of the sensor during sealing. It is felt that these areas may form leakage paths due to uneven coating. In addition, special sensors have been fabricated that are used as electrodes in saline tests. These electrodes more accurately duplicate the actual pressure transducer.

It appears at this time that because of temperature and hysteresis problems, polyurethane and parylene will be unacceptable coating materials, as is the silicon filled epoxy. The Kraton polymers have very good properties and can be used if the application problems can be solved. The silicone rubbers, however, show the most promise for immediate applications. Teflon also merits further work, and some consultation with Lewis Research may be done.

Future work will include long-term testing in saline to determine lifetime and stability. Tests on accelerated aging due to heat are being started. A protocol for testing and evaluation of materials is being formulated.
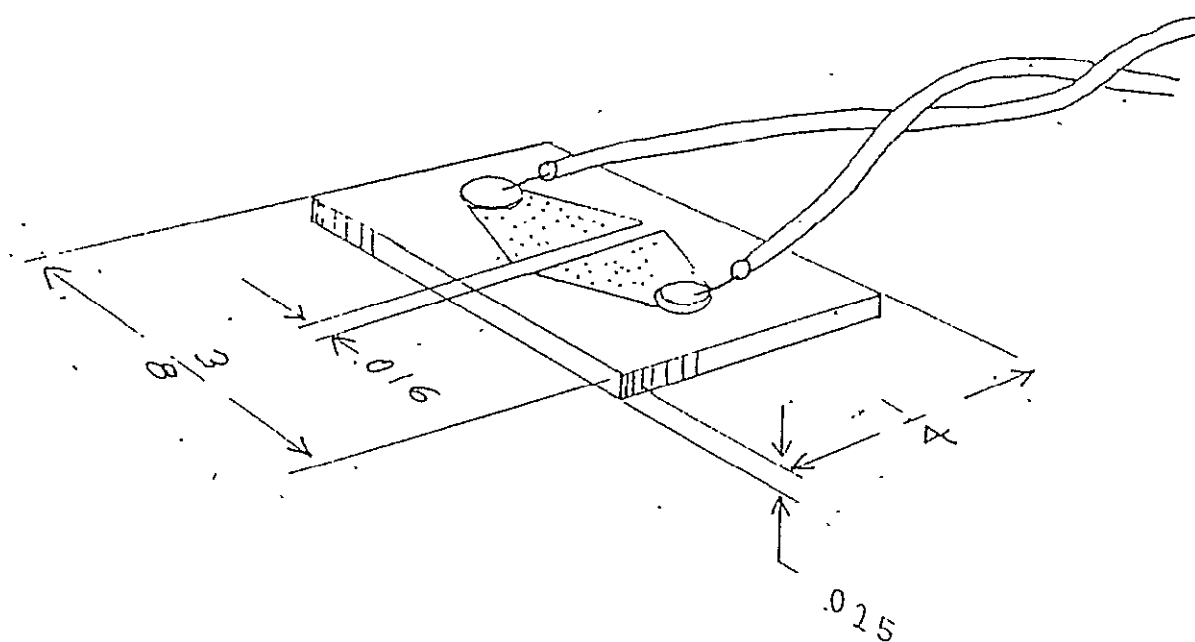
FIGURE D-1

Goodyear	Time to Failure		8/4/75	Time to Failur
41	46 days	96	EP 40%	70 days
42	46 days	97	EP 40%	77 days
		98	EP 35%	
43	8 days	99	EP 35%	77 days
44	10 days	100	EP 35%	70 days
		101	EP 35%	12 days
Vorite			9/15/75	
51 EP 54%	32 days	102	EP 45%	2 days
52 EP 54%	>100 days T	103	EP 45%	2 days
53 DB 58%	>100 days T	104	EP 45%	3 hours
54 DB 58%	35 days	105	DB 42%	3 hours
55 DB 60%	>100 days	106	DB 42%	3 hours
56 DB 60%	4 hours	107	DB 45%	2 days
57 DB 60%	>100 days T	108	DB 45%	2 days
58 DB 60%	60 days	109	DB 47%	2 days
86 DB 60%	7 days	110	DB 47%	10 minutes
87 DB 60%	7 days	111	DB 50%	2 days
88 DB 58%	90 min.	112	DB 50%	2 days
89 DB 58%	4 days	113	DB 50%	10 minutes
90 DB 54%	35 days	114	DB 50%	8 days
91	6 hours		9/29/75	
7/15/75		115	DB 50%	15 days
93 DB 60%		116	DB 50%	15 days
94 DB 60	75 days	117	DB 50%	30 days
95 DB 60		118	DB 50%	15 days

Diaphragms 10/7/75

22 DB 50%

23 DB 50%   28 days

Sensors

32 Goodyear   30 minutes
53 Goodyear   5 days
55 Goodyear   15 days

POLYURETHANE MATERIALS

Diaphragms	Time to failure
10/20/75	
27 DB 50%	30 days
28 DB 50%	30 days
29 DB 50%	

Sensors

10/22/75

CD 7   DB 50% and Polyethylene tube
CD 9   DB 50% and Polyethylene tube

	5/22/75 Diaphragms	Time to Failure
57	NIH .25 mils	5 days
58	"	5 days
59	"	5 days
60	" Primer	18 hours
61.	" Primer	5 days

	9/22/75 sensors 38°C saline	
11	U.C. 4mils	43 days
14	"	17 days
17	"	

	10/1/75 diaphragms 50° saline	
A	U.C. 4 mils	2 days
B	"	2 days
C	"	14 days
D	"	22 days

Epcar 847		Time to Failure
29	10 mils	64 days
30	"	8 days
31	"	90 minutes
32	"	20 days
33	"	19 days
34	"	34 days
35	"	40 days
36		30 days
37		100 days T
38		100 days T

5/8/75

59	100 days T
60	6 hours
61	21 days
62	1 day
63	72 days
64	35 days

10/19/75

133	8 days
134	90 minutes
135	2 days
136	8 days

Sensors

VS 18 Epcar	5 minutes
VS 19 Epcar	6 minutes

Diaphragms
10/20/75

34	Kraton	22 days
35	Kraton	2 days

Kraton		Time to Failure
4A		300 days
4B		119 days
4C		>250 days T
4D		>250 days T
4E		>250 days T
4F		>250 days T
5A	10mils	104 days
5B		45 minutes
5C	20mils	156 days
5D		176 days
5E	40mils	81 days
6A		0 days
6B		12 hours
6C		166 days
6D		90 days
6E		82 days
6F		225 days T

21 over Epoxy	19 days
22	21 days
23	19 days
24	12 days

25 over wax	>200 days
26	135 days

27	>200 days
28	>200 days

10/19/75

125	1 day
126	30 minutes
127	30 minutes
128	4 days
129	1 days
130	90 minutes
131	15 minutes
132	1 day

11/17/75

Time to Failure

156	5 dips	
157	5 dips	
158	5 dips	1 day
159	5 dips	2 days
160	5 dips	30 minutes
161	5 dips	15 minutes
162	5 dips	1 day

Polycrystalline silicon in Hysol RS-2038 Epoxy

Diaphragms . Time to Failure

0 .. 12 days
1 · 12 days

10/7/75
24 13 days .
25 15 days
26 . 14 days

A-11

4/28/75   Time to Failure .

45	Dow 630	45 minutes
46	Dow 630	4 hours
47	Dow 1890	>100 days T
48	Dow 1890	>100 days T
49	Dow 3140 RTV	>100 days T
50	Dow 3140 RTV	>100 days T

5/27/75

79	1890	>100 days T
80	1890	>100 days T
81	1890	>100 days T

10/19/75

121	3140 RTV
122	3140 RTV
123	3140 RTV
124	3140 RTV

Diaphragms

S1	Silastic·Polyethylene tube	8 hours
S2	3140 Polyethylene tube	20 days
S6	3140 & Primer Polyethylene tube	15 days

10/7/75

| 21 | 3140 & Polyethylene tube |

10/20/75

30	3140 & Polyethylene tube	
31	3140 & Polyethylene tube	
32	3140 & Polyethylene tube	52 days

Sensors
10/22/75

| CD 4 | 3140 and Silastic tube |
| CD 5 | 3140 and Silastic tube |

A-12

POLYETHYLENE

10/30/75		Time to Failure
137	2 coats	5 minutes
138	2 coats	5 minutes
139	2 coats	5 minutes
140	4 coats	
141	4 coats	
142	4 coats	
143	3 coats	20 minutes
144	3 coats	15 minutes
145	3 coats	10 minutes

11/5/75		
146	5 coats	6 days
147	5 coats	6 days
148	5 coats	1 hour
149	6 coats	6 days
150	6 coats	1 day
151	6 coats	2 hours
152	6 coats	5 days

A-13

A SINGLE FREQUENCY RF POWERED THREE CHANNEL TELEMETRY SYSTEM

Introduction

·Because of the relative   large size and limited lifetime of conventional battery power, RF has become a very promising means of powering implant units and hence has been extensively studied during the past years. This telemetry system stemmed from the single channel RF powered telemetry system developed here in MEL. In this part- icular application, a single coil in the implant unit was used for both RF energy absorption and signal transmission and therefore reduces the space needed for the two-coil system - one for RF powering and another for signal transmitting at differ- ent frequencies. A time sharing multiplexing technique was used.

The physiological events intended to be monitored includes aortic blood pressure, body temperature and electrocardiograms. Aortic pressure normally requires a frequency range of about 40 Hz for meaningful recording, EKG needs about 80 Hz; while body temperature is understood to be a very slow varying parameter. Work up to now has included the system circuit design and system performance to bench stimulation. The remaining problem lies in the packaging area and further investi- gation is being carried out.

System description

A system block diagram is shown in Fig. D- 1. Pulse position modulation is used for coding the information. Since the same frequency is used for RF powering and signal transmitting, signal received by the demodulation unit will also consist of these two components. The signal format is shown in Fig. D- 2.

· Fig. D- 2.

A-14

```
┌─────────┐
│    1    │────┐
└─────────┘    │
               │     ┌──────────────┐      ┌──────────────┐
┌─────────┐    │     │  Multiplexer │      │              │        ╭───────╮
│    2    │────┼─────┤      &       │──────┤  Transmitter │────────│       │
└─────────┘    │     │  Modulator   │      │              │        ╰───────╯
               │     └──────────────┘      └──────────────┘
┌─────────┐    │
│    3    │────┘
└─────────┘
```

Transducer & Amp.

```
                                               Y
                                               │
┌──────────────┐    ╭───────╮                  │     ┌──────────────────┐
│              │    │       │                  │     │   Receiver   &    │──○
│  RF powering │────│       │                  └─────┤   demodulation   │──○
│              │    ╰───────╯                        │                  │──○
└──────┬───────┘                                     └─────────┬────────┘
       │                    ┌──────────────────┐               │
       └────────────────────┤  Synchronization ├───────────────┘
                            └──────────────────┘
```
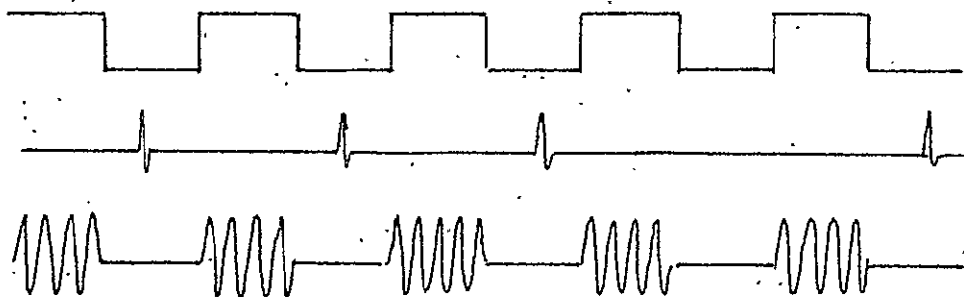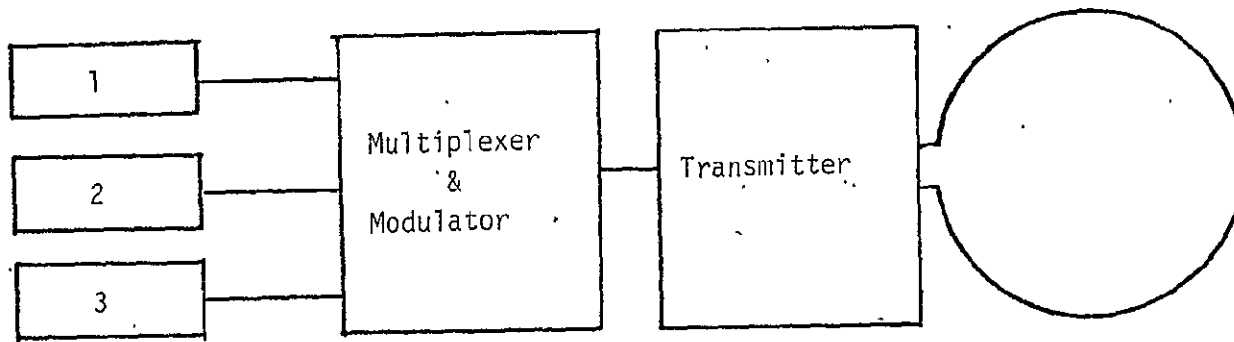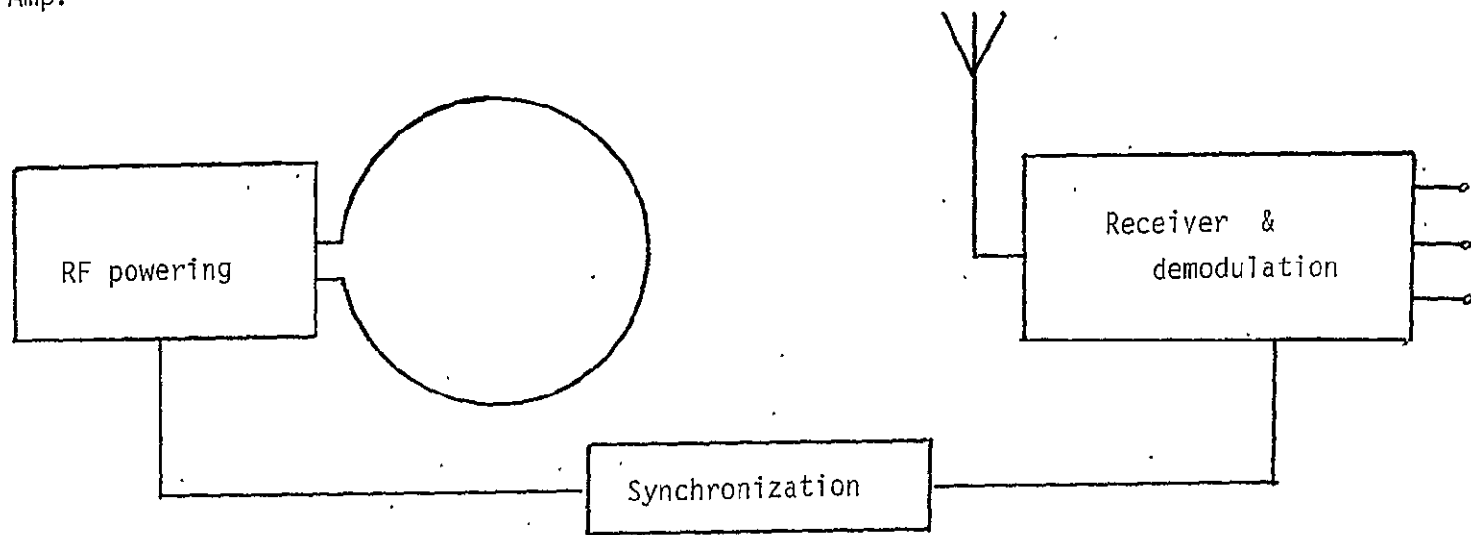
Fig D-1. System block diagram

The entire system is synchronized by a clock, as shown in the upper trace. Three sequencing channels are followed by an "empty" channel for channel synchronization purposes. Time lapse between the falling edge of the clock pulse and the signal pulse will then represent the informations -- t_1, t_2 and t_3 in the middle trace. RF powering is delivered during the high periods of the clock as shown in the bottom trace.

The entire system can be divided into an implant unit including transducers, amplifiers, modulator and transmitter; and an external unit which includes the RF powering unit and demodulation unit. They will be discussed separately:

Implant unit. (Fig. D-1)

        The Implant unit includes the transducers, transducer amplifiers, modulator and transmitter.

(1) Modulator and transmitter.

The modulator is in fact a voltage-to-pulse position converter, the output of which then activates the transmitter. The circuit is shown in Fig. D-3, and the timing diagram in Fig. D-4. In order to avoid the inter-channel influence, a 470 pF capacitor will be clamped to V+ at every "HI" period of the synchronization clock, through the fourth channel of the 14016 analog gate. The current source for the 470 pF capacitor consists of two 2N3906 transistors shown on top of the capacitor in the diagram.

Fig. D-5. shows the circuit diagram of the transmitter, which also acts as the RF power detector. A MPF102 N-channel FET serves as the rectifying diode during RF period. The Copttis oscillator is activated by pulses from modulator. Clock filtering is achieved through diode detector on the left side of the coil in Fig. D-5. Voltage step down is necessary because of the strong RF induced clock peak-to-peak voltage.

(2) Transducer and transducer amplifier.

Since the pulse position information results from a voltage-to-pulse position conversion, truthful transduction of a physiological event into voltage for the conversion is essential. However, since it is an implant unit; size, power consumption and circuit complexity all have to be taken into account. A compromise of all these concerns will be used to select the final design. For temperature sensing, a YSI thermister (part #44015) with a resistance value of 547K ohms at 37°C is used. The basic idea of the circuit for transduction is that by using the Op. Amp. A1
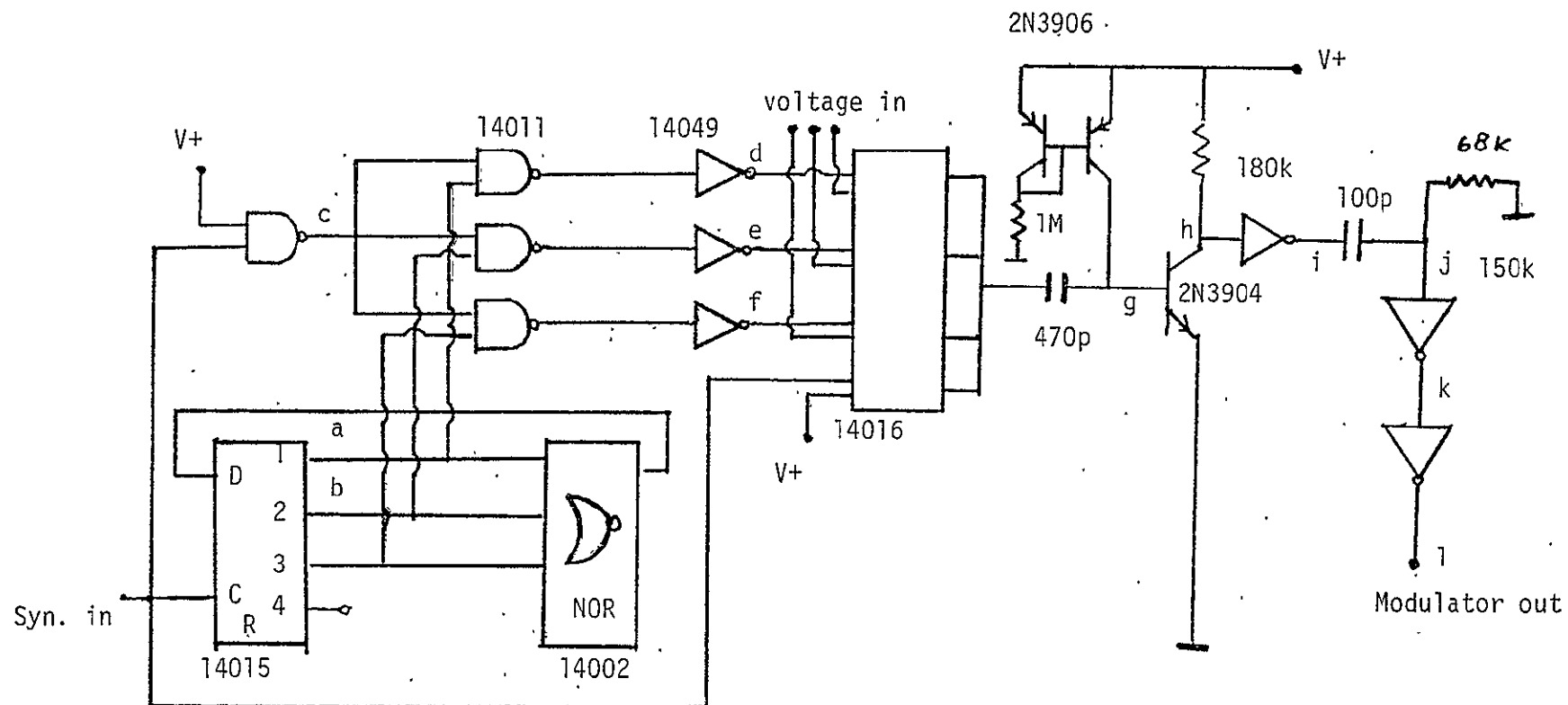
Fig. D-3 Modulator - a voltage-to-pulse position converter
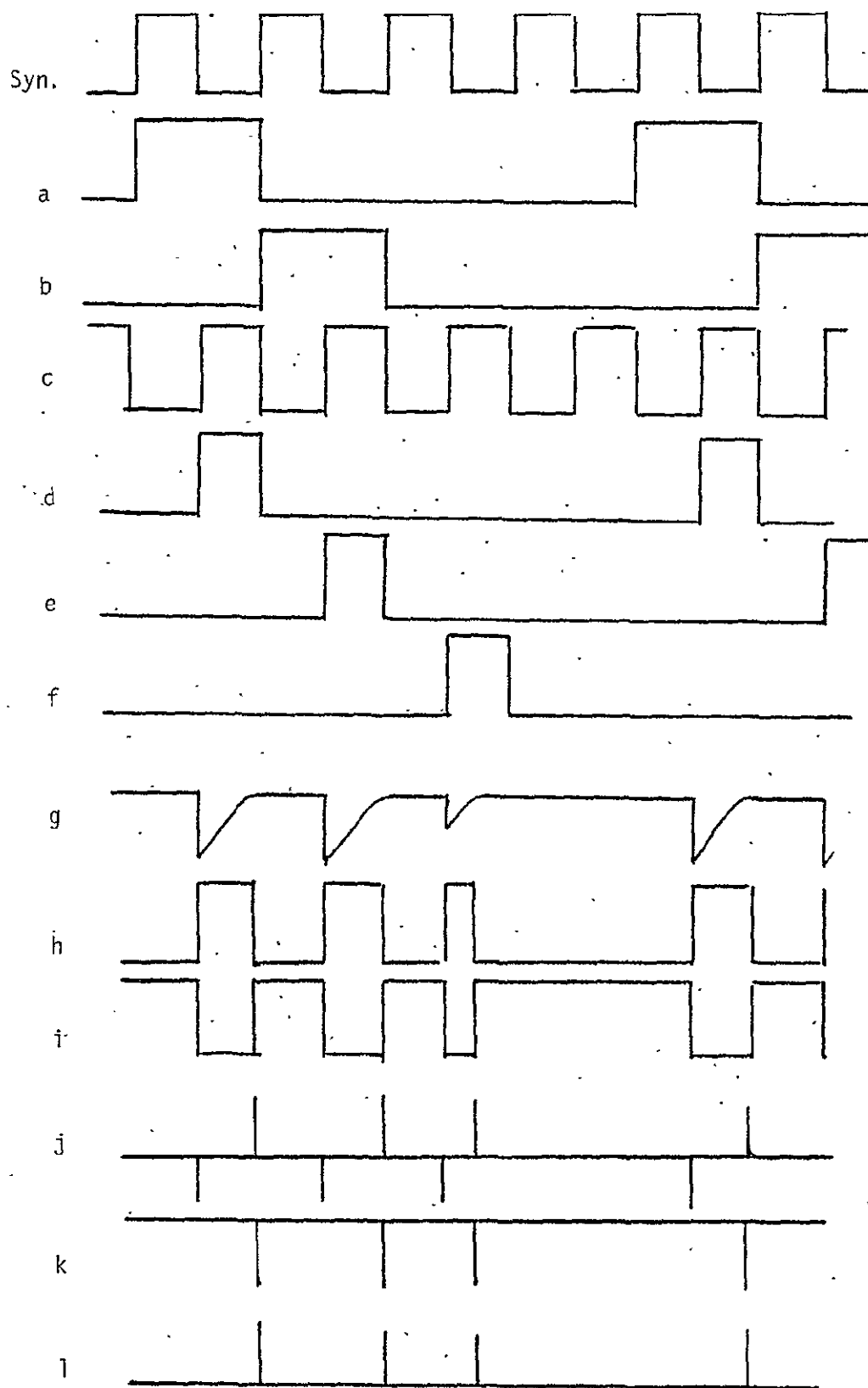
Fig. D-4. Timing for modulator

A-18
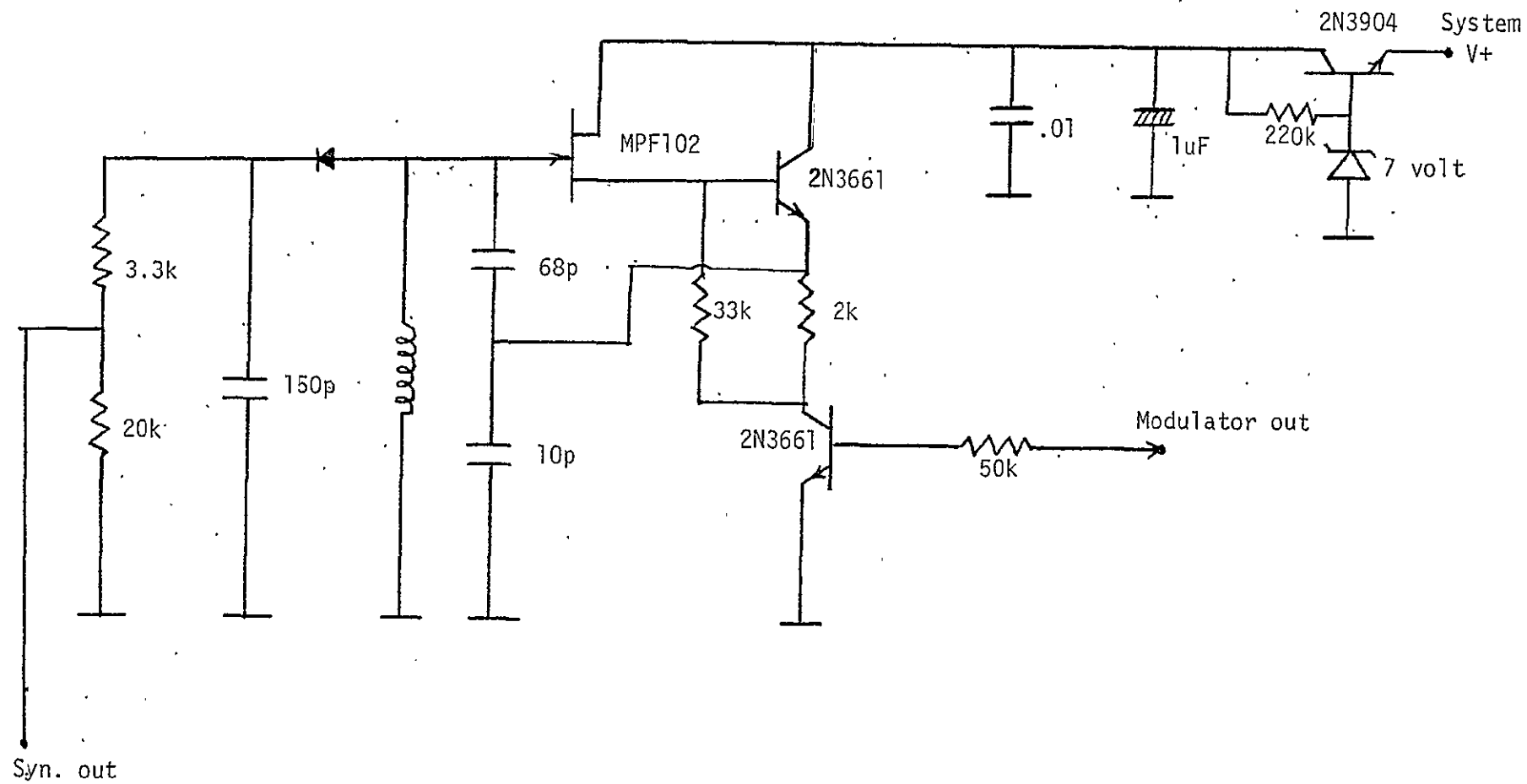
Fig. D-5 - RF Transmitter and power detecting circuit

(Fig. D- 7) as a constant current source, a very linear temperature-to-voltage con-
version can then be generated across the feed-back loop in the range of 32° to 43°C.
Op.Amp. 2 is used only for amplification and output voltage adjusting purposes. A
possible error may occur from the power supply temperature coefficient. However,
according to the circuit analysis, $\frac{d\ e1}{dVcc}$ is around 0.5. By using a 2N3904 transistor
base-emitter reverse breakdown voltage as the power supply regulator, we experienced
a temperature coefficient of Vcc around 40 mV over a range of 10°C or about 0.5mV
for 0.1°C change(refer to Fig. D-6). With the temperature sensitivity of 22 mV/.1°C,
assuming an ideal power supply, obtained from the amplifier output e2, one can see
that this change due to regulator's temperature coefficient, reflecting at.C2 after
the second stage amplification of 10, is about 2.5 mV/.1°C and will not be an
intolerable problem. When it is also remembered that this temperature effect tends
to linearize the thermister's non-linearity at the higher portion of the temperature
range, as well as the fact that calibration is done after the demodulation, this
temperature effect due to the power supply is not a problem.
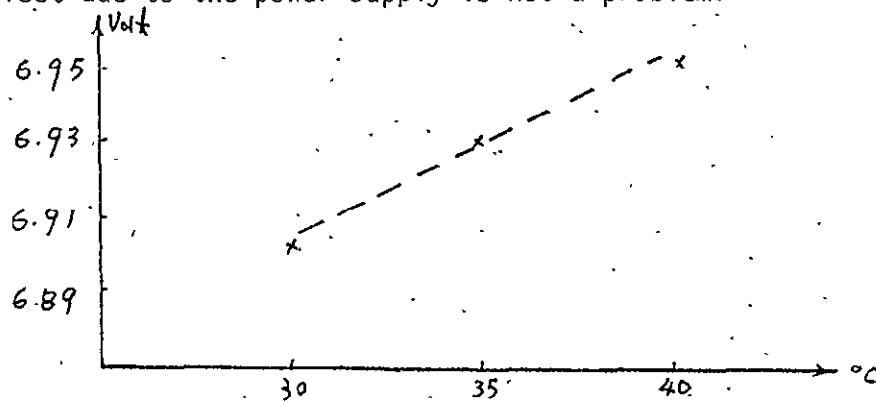
Fig. D- 6

Fig. D-8 shows the amplifier's output voltage plotted against temperature. A good
linearity can be observed.

More efforts have expended into the pressure transduction. A small size semi-
conductor bridge pressure sensor developed in MEL is used for pressure measurement.
The amplifier diagram is shown in Fig. D-9. A high input impedance amplifier is used
for amplification to avoid any loading on the bridge. However, due to the limitation
of the RF power source and the low sensitivity with the present semiconductor sensor,
a "pulsing" technique has to be utilized to provide a workable signal while keeping
the power consumption within range. In other words, the bridge sensor is excited
non-continuously during a particular period of time with relatively high current.
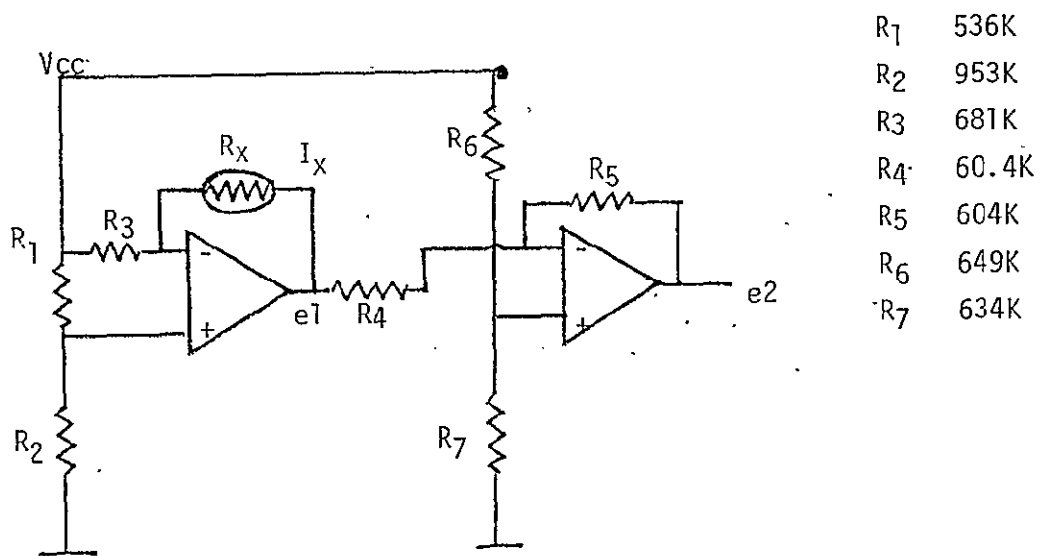
Fig. D-7 Temperature sensing amplifier

R_1	536K
R_2	953K
R_3	681K
R_4	60.4K
R_5	604K
R_6	649K
R_7	634K
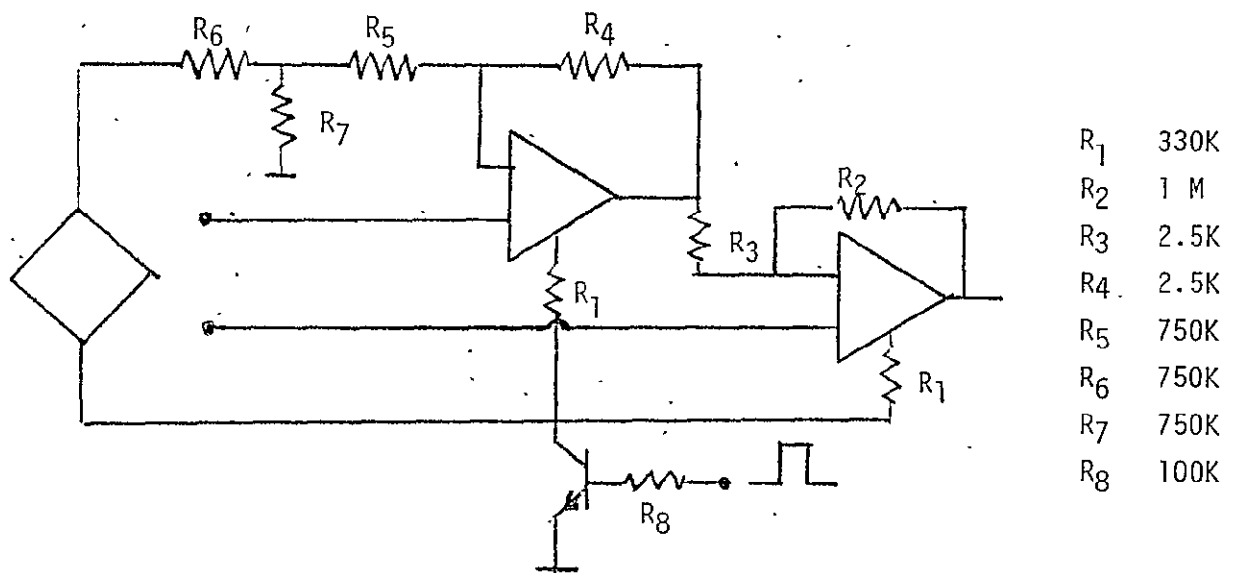
Fig. D-9 Pressure sensing amplifier

R_1	330K
R_2	1 M
R_3	2.5K
R_4	2.5K
R_5	750K
R_6	750K
R_7	750K
R_8	100K
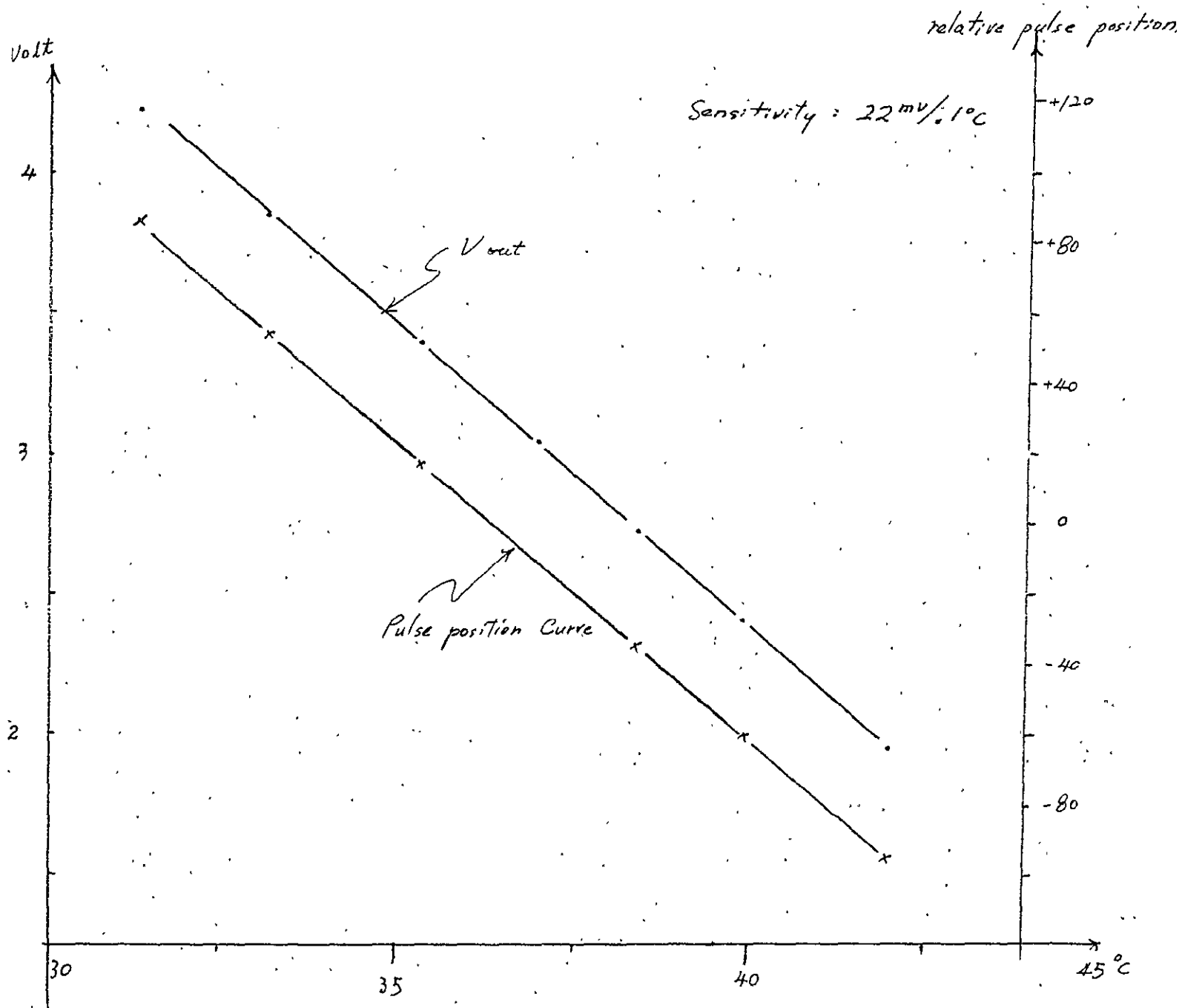
FIGURE D-8

Sampling and holding is also achieved during this period. Timing for the bridge pulsing is shown below in Fig.D-10.
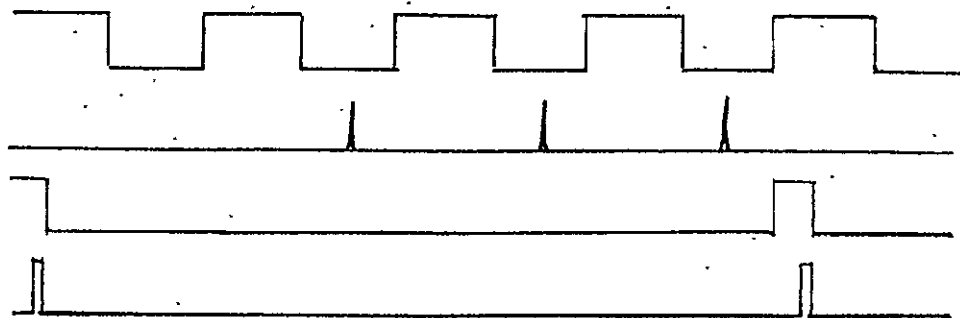
Fig. D-10

The pulsing achieved at the synchronous pulse stemmed from the rising edge of this pulse. The bridge's power pulse length is about 100 μsec and the excitation current through the bridge is about 3 mA. A sampling window is opened at the end of this pulse and is about 15 μsec. Pulsing again is applied to the I-set terminal of the amplifier to obtain a fast settling time of the amplifier. Although with this I-set value, the Op. Amp. has a small signal gain band-width product of about 100 KHz, the measured large signal gain bandwidth product is only around 6 to 8 KHz. In view of any sudden disturbance that might occur in the pressure, which may represent a large signal rather than a small one, the amplification of the amplifier is restricted to about 400. The output swing voltage for 200 mmHg ranges about 2 volts. Fig. D-11 shows the switching for bridge pulsing and Fig. D-12 gives the amplifier's output plotted against 200 mmHg pressure range. The significance of the temperature influence on the transducer can also be seen from this data. The compensation of the temperature effect will be discussed later.

The EKG amplifier is shown in Fig. D-13. and is a conventional design.

External Unit

Demodulation and RF powering.

(1) Demodulation.

The signal received by the receiver, as mentioned, consists of the information signal and RF signal. The format is shown below:
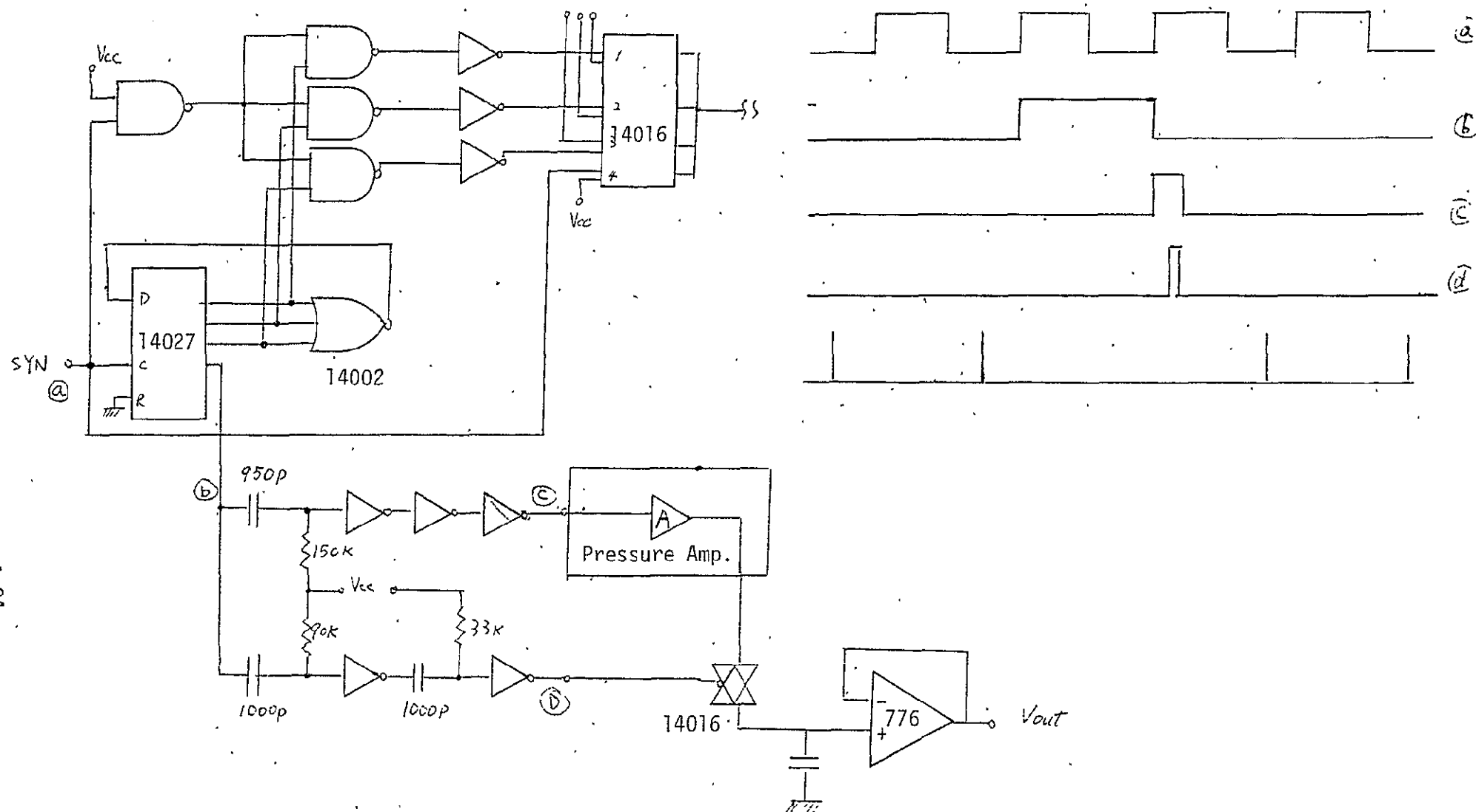
Fig.D-11 Logic and timing diagram for bridge pulsing
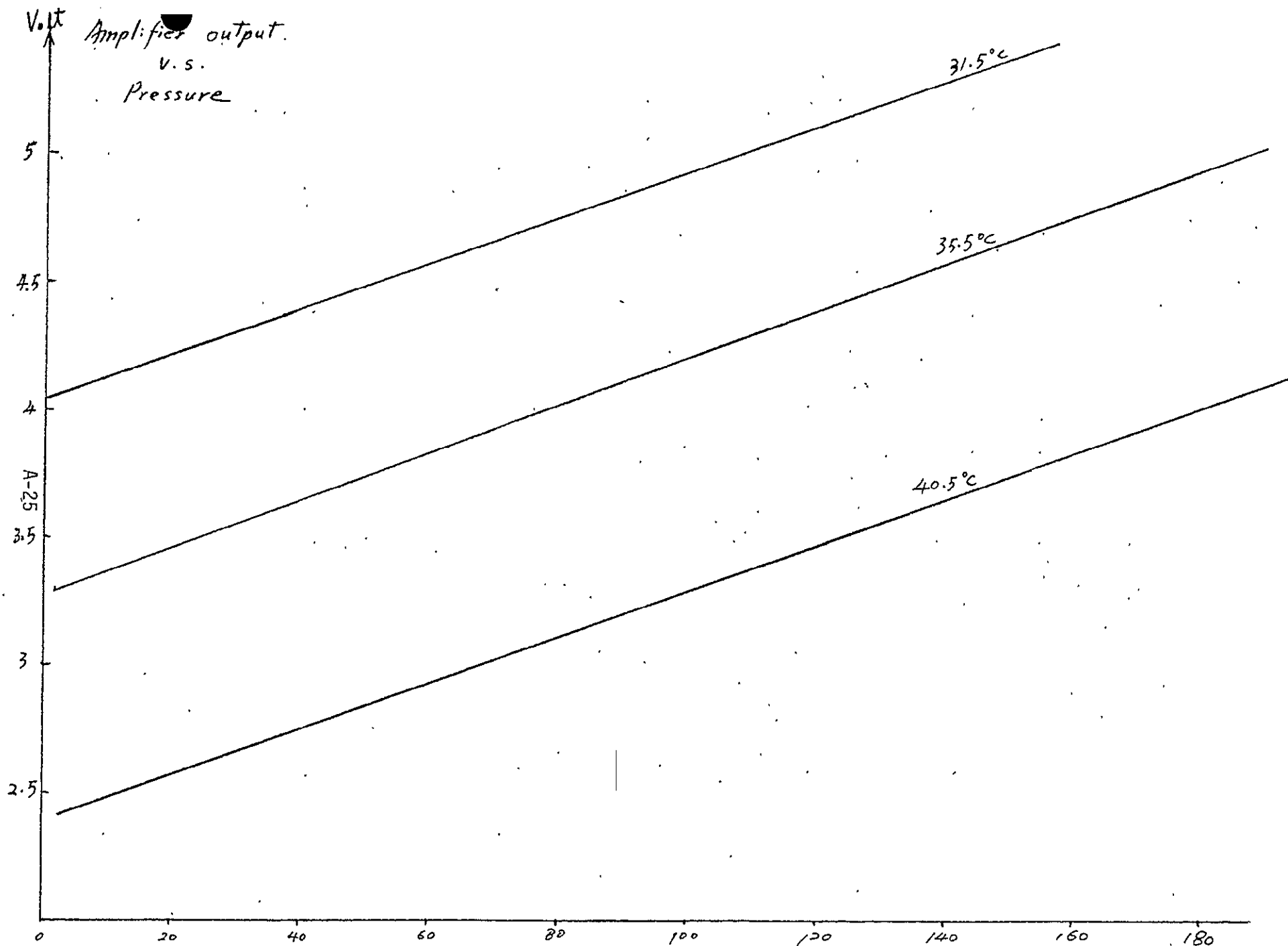
FIGURE D-12
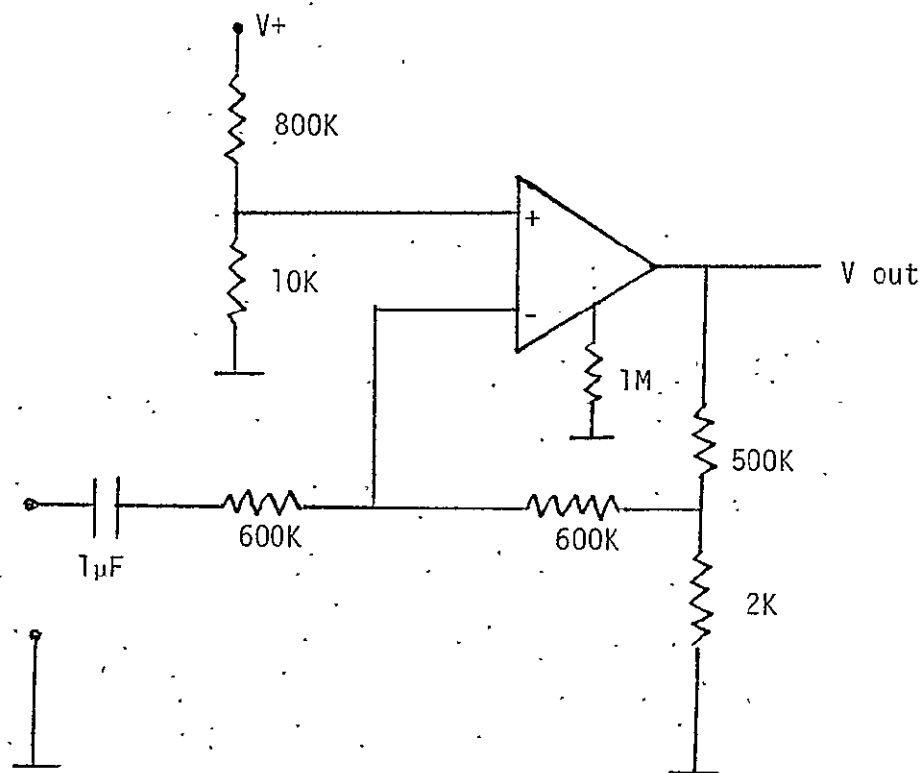
Fig. D-13   EKG Amplifier

Multiplexing of the channel is sequential and the period marked "p" is the RF signal.

The block diagram for demodulation is shown in Fig. D-14. The function of the individual blocks are described as follows:

Antenna switch. As transmitting and powering are at the same frequency, a great amplitude difference between these two signal sources exists and protection of the AM receiver is necessary. This is achieved by attenuating the RF powering signal received by the antenna with a switching circuit (the circuit is shown in Fig.D-15.). The control for switching is shown in Fig. D-16. Control pulses are generated from the clock. The format is as follows:
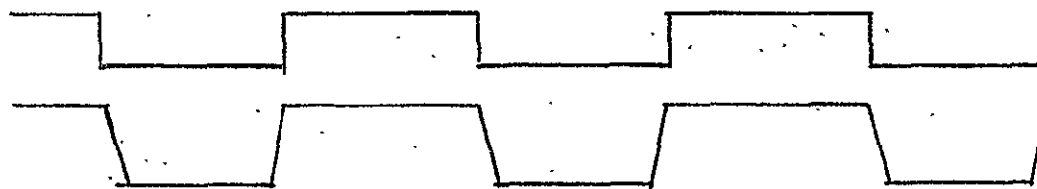
The n-channel MPF102 FET has a typical "ON" resistance at zero gate voltage of about 700 ohms channel resistance; and the typical "OFF" resistance at -7 volts is over 5 M ohms. When the control pulses go to low(-7 volts) level, n-channel FET MPF 102 is turned OFF;while p-channel enhancement mode MOSFET is ON. Conversely, at zero gate voltage the P channel enhancement mode MOSFET has a typical "OFF" channel resistance of greater than 100 M ohms and an "ON" resistance at -7 volts of less than 0.5 K ohms. Consequently, the signal received by the antenna will be attenuated when delivered to the receiver through this circuit if the applied gate voltage to the two FETs is at zero volts, which in this case occurs during the RF powering period. The attenuation was previously measured at about -90dB.

Threshold detector.- Fig. D-17. This circuit serves both as a threshold detector and pulse level shifter - due to the fact that the synchronous clock and receiving signal pulses are 0 to Vcc peak-to-peak while the signal processing units operated at $\pm$Vcc. The purpose of this detector is to minimize the noise resulting from transmitting and receiving process. A one shot is followed to adjust the pulse width according to the sampling requirement. The present pulse width is set at 12 μsec.

Signal before
Threshold detector

Signal after
Threshold detector
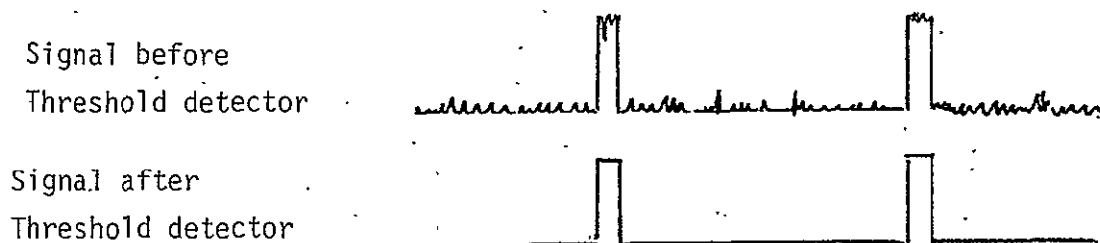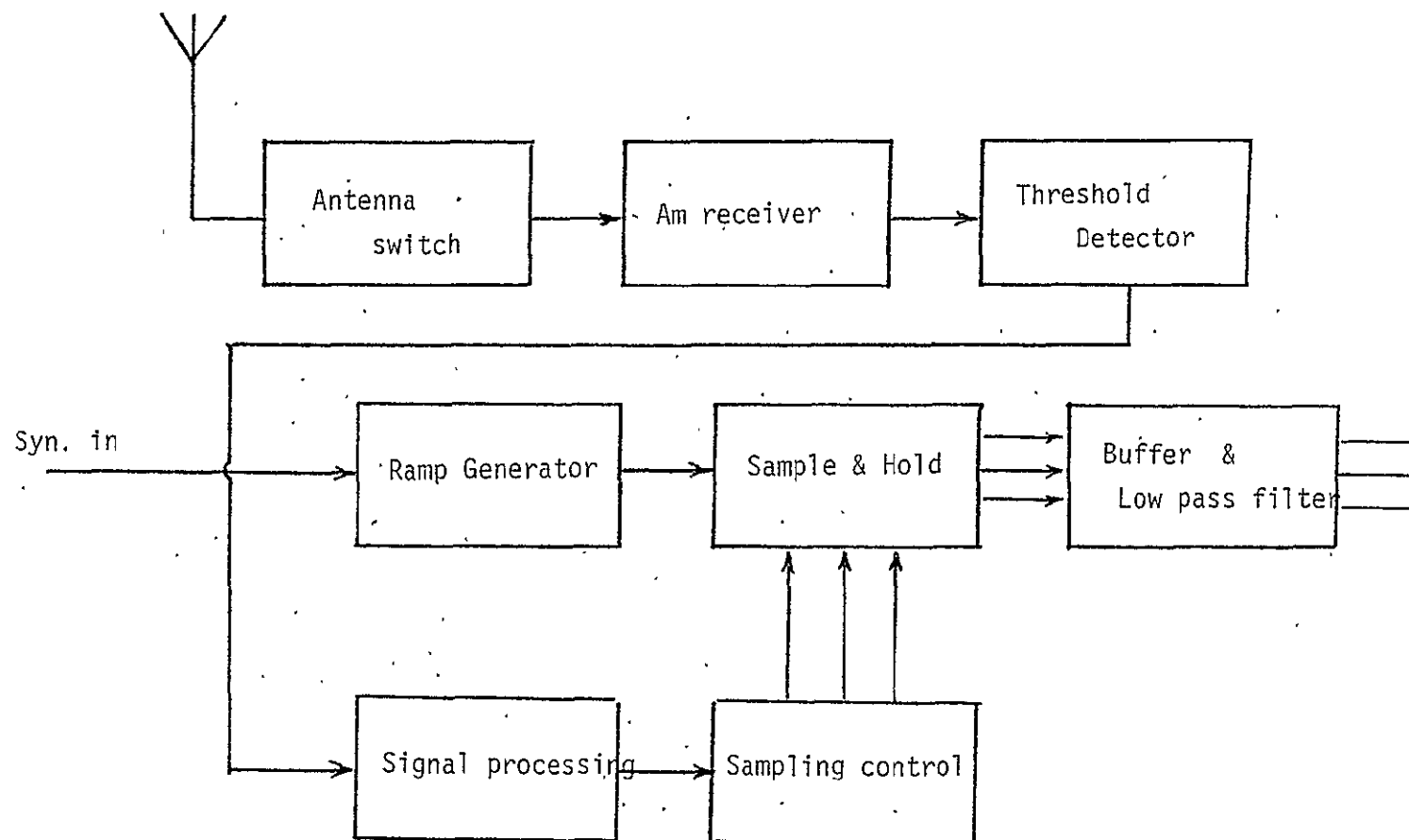
Fig. D-18

Fig. D-14   Demodulation block diagram
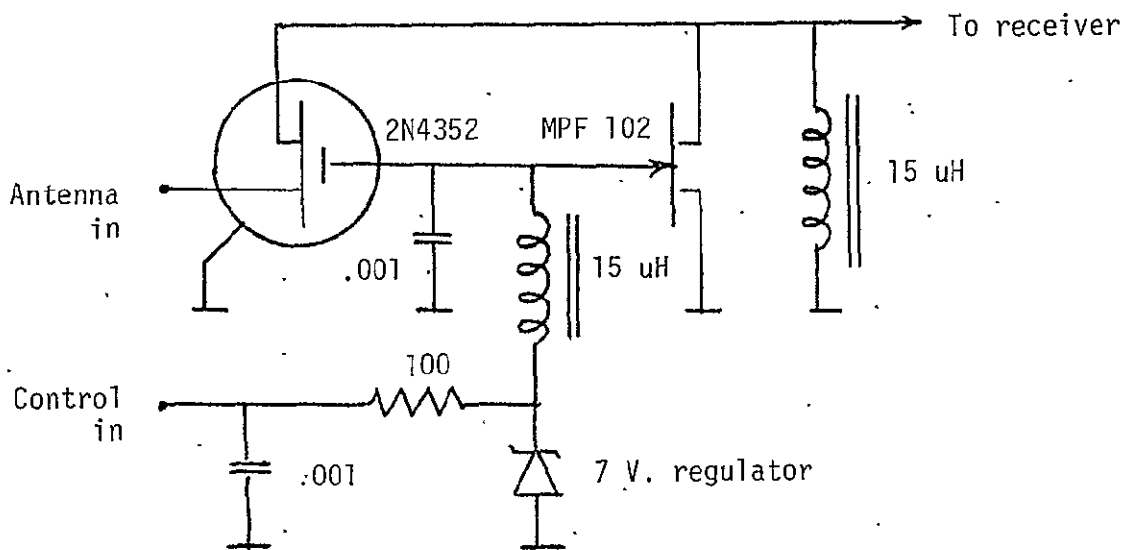
Fig D-15   Antenna switch
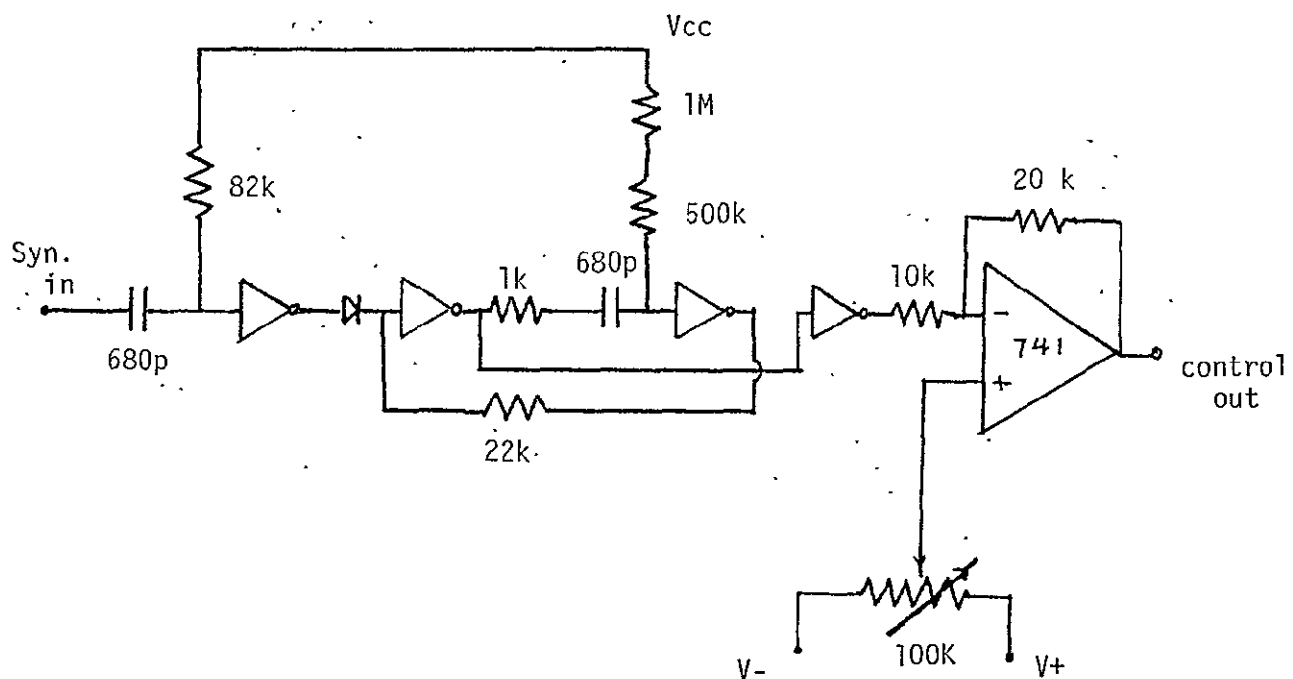
Fig. D-16   Antenna switch control
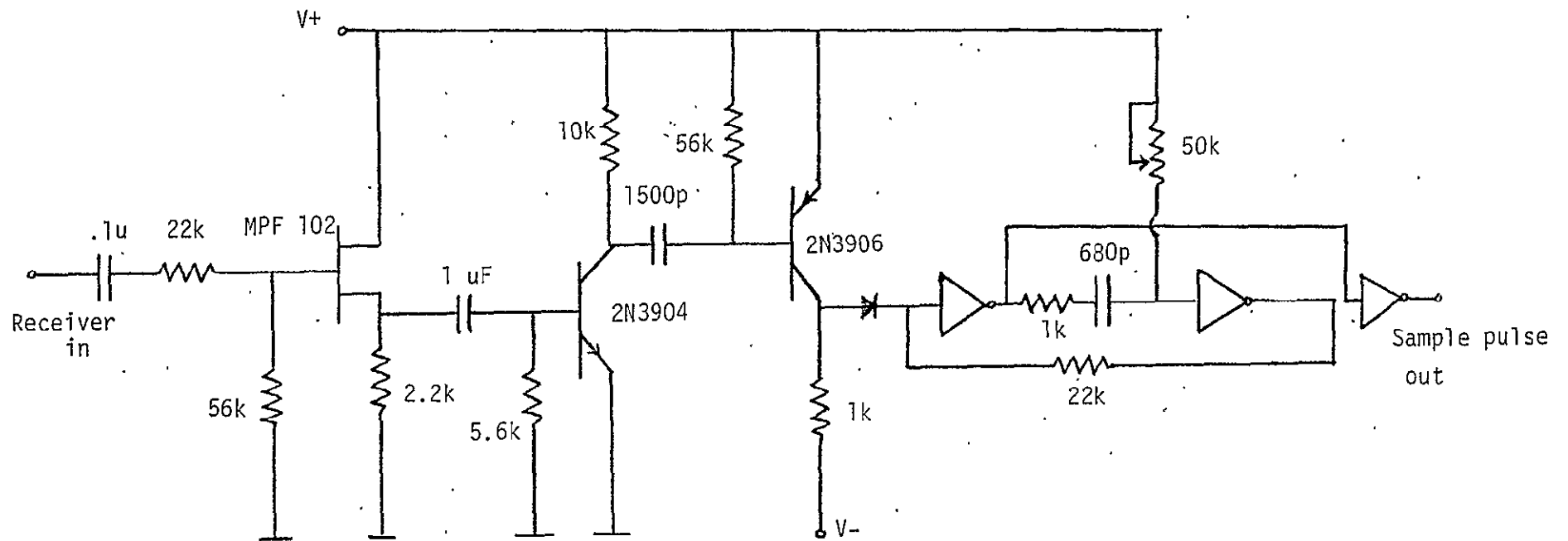
Fig. D-17   Threshold detector

Ramp generator: Information will be recovered from pulse position coding by sampling the voltage along a ramp.
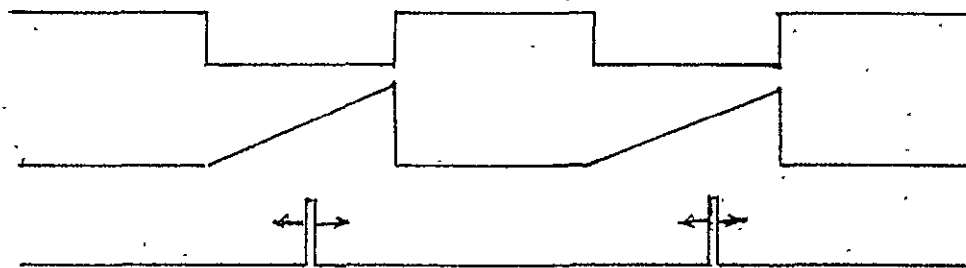
Fig. D-19

The ramp generator circuit is shown in Fig. D-20. and it uses the stable zener diode functioning voltage as a reference for the constant current supply source to charge the capacitor over the feedback loop. From the circuit analysis, the ratio between the zener's dynamic resistance (R_{dyn}.) and R_1 (refer to Fig. D-20), R_1/R_{dyn}, should ideally be as large as possible. This means that for each practical zener, only one optimum operating point is available. The zener presently used is a LM 103 2.4 volt regulator which has a very low R_{dyn} in the range $10.\mu a$ to 10 ma.

Signal Processing. This part converts the sequencing pulse signal into three independent channel pulses. A CMOS logic device is also used here. The circuit is shown in Fig. D- 21 and the timing diagram in Fig. D- 22. Since any signal in the RF period represents errors, that period is blocked totally.

Sampling, holding and buffer stage. - Fig. D- 23. An analog gate is used for sampling; activated by the sampling pulse resulting from the signal processing block. The CMOS 14016 analog gate has an "ON" resistance of about 400Ω and very high "OFF" resistance. The input - output delay time is in the nanosec range. The holding capacitor is 4700 pF, which during sampling gives an RC constant of about 2 μsec. The sampling time, as previously mentioned, is 12 μsec. For the buffering stage, a 2H0042 FET Op. Amp is chosen because of its 10^{12} Ω input resistance and very low input bias current. A low pass filter with a high-cutoff at 120 Hz is followed to the buffer stage.

Clock. The clock is generated by a 555 timer, shown in Fig. D-24. The present clock rate is set at 800 Hz, which gives a 200/sec sampling rate for each channel.

(2) RF Powering

The power for the implant unit is supplied by RF induction from a primary coil, which is the external unit, into the secondary coil, which is also the implant unit's
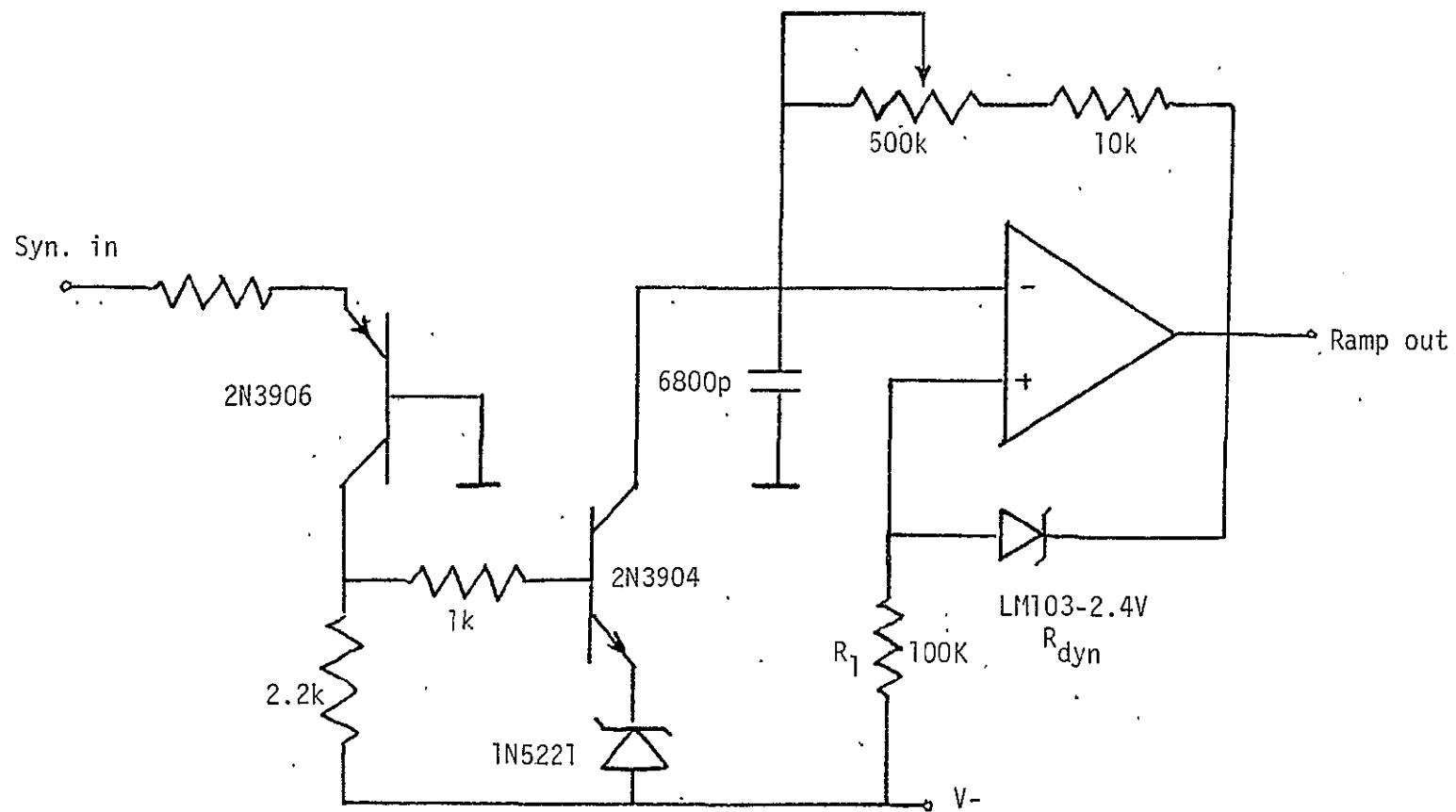
Fig. D-20 Ramp generator
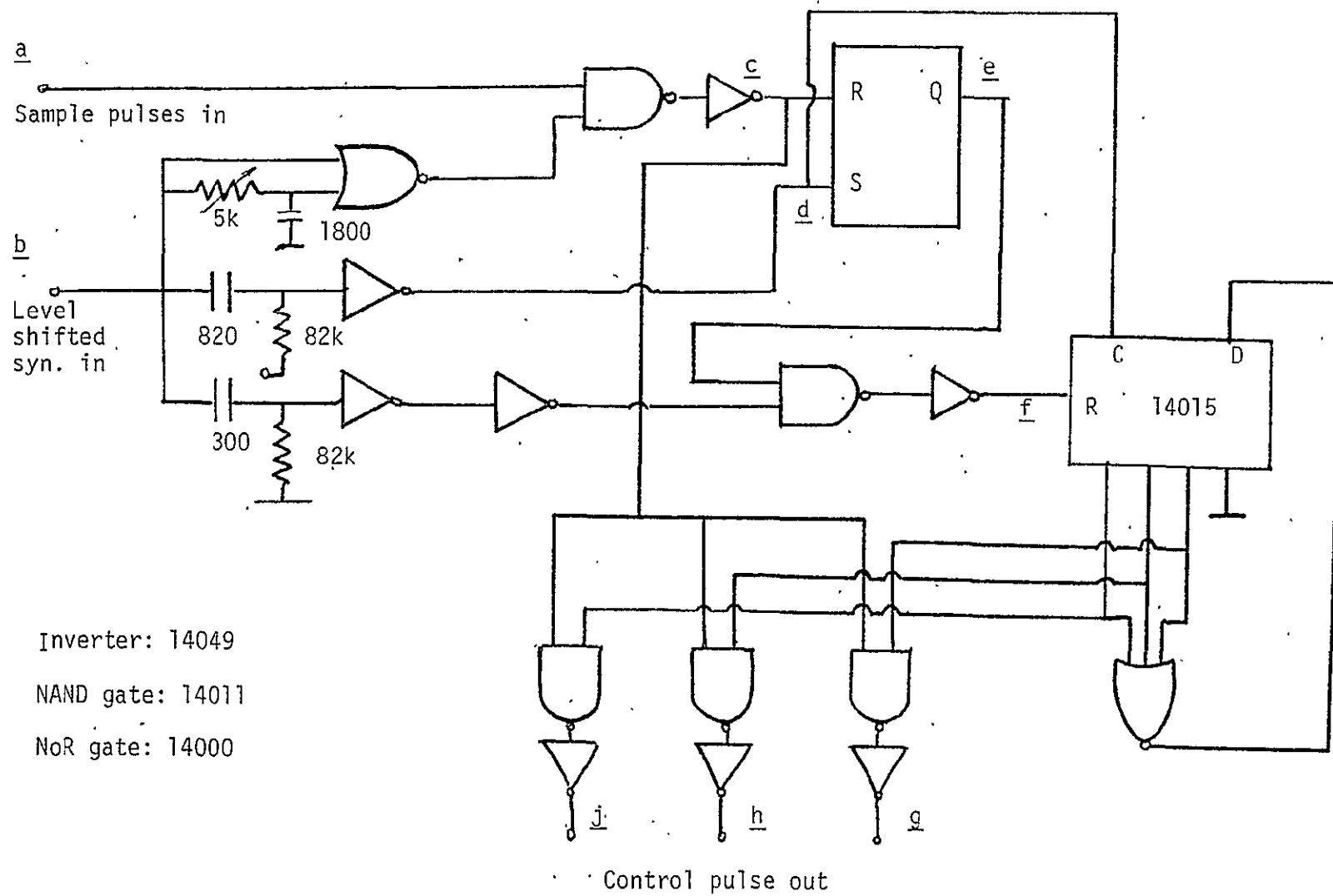
Fig. D-21   Signal processing unit

a

+7.5V
-7.5V

b

c

d

e

f

g

h

j

Ramp

........+4V

...-4V

Fig. D-22

control pulses in

Ramp in

14016 analog gate

4700p x 3

LM310 x 3

1k   1uF

output
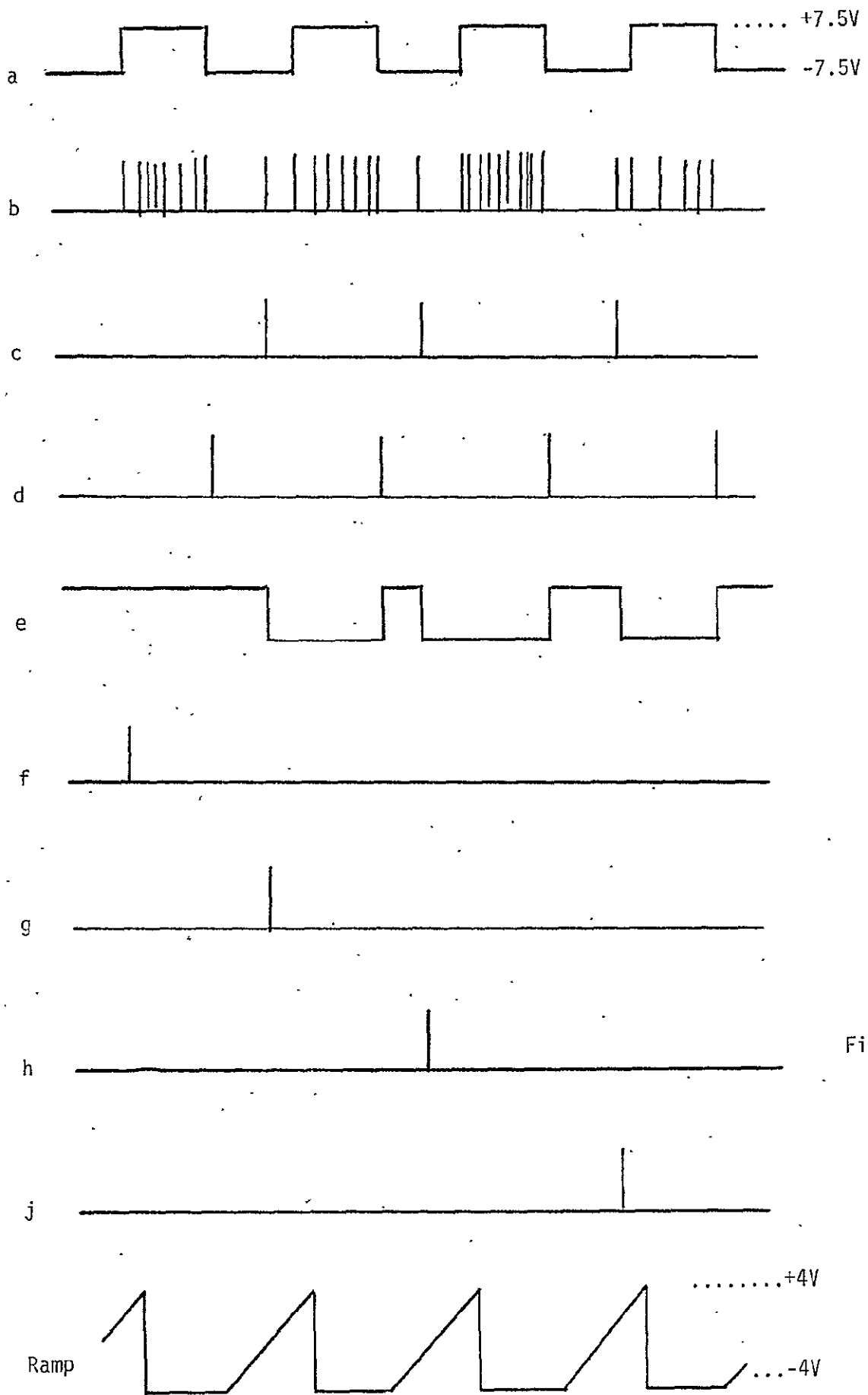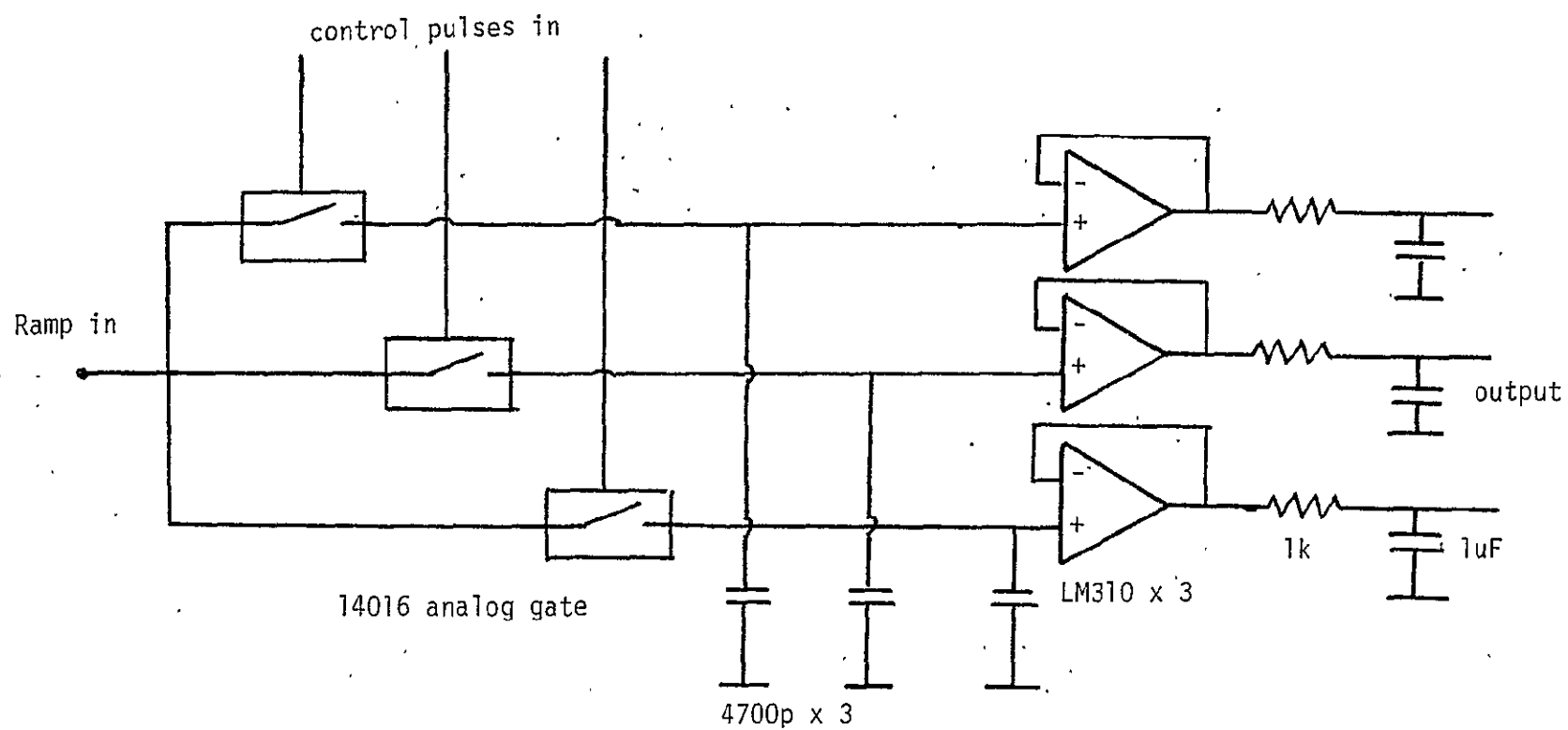
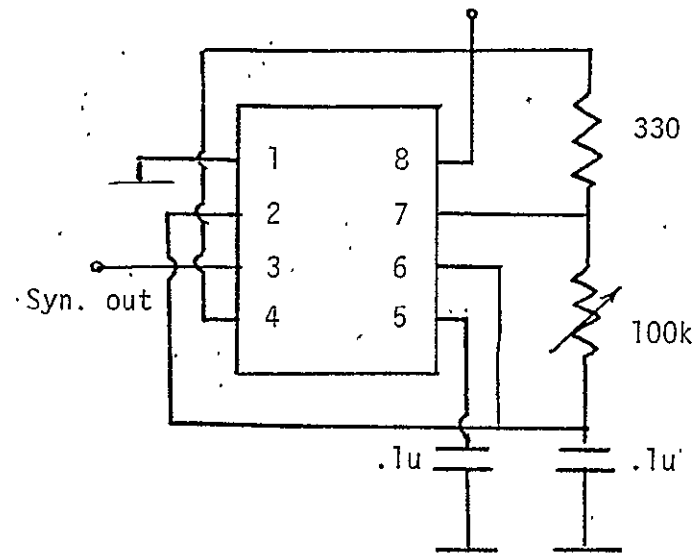Fig. D-23   Sampling, holding and buffer stage

Fig. D-24   Clock generating

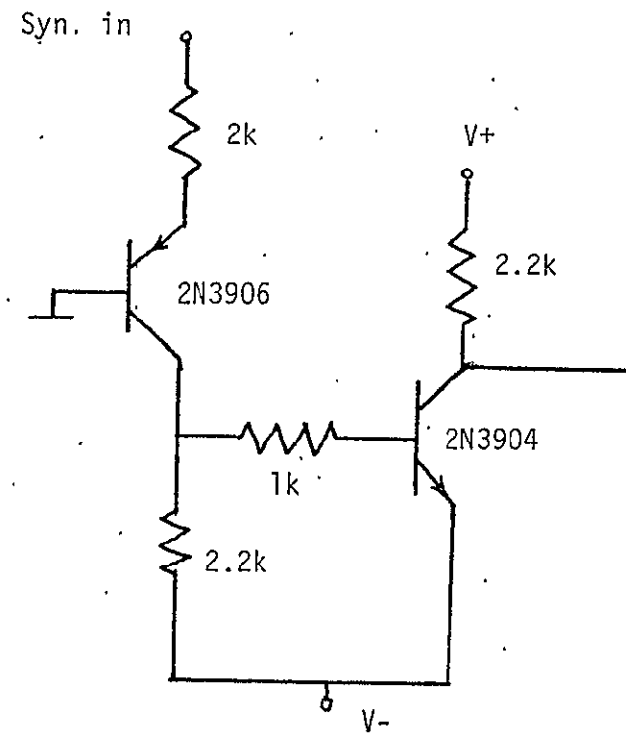Fig. D-25   Syn. level shifting
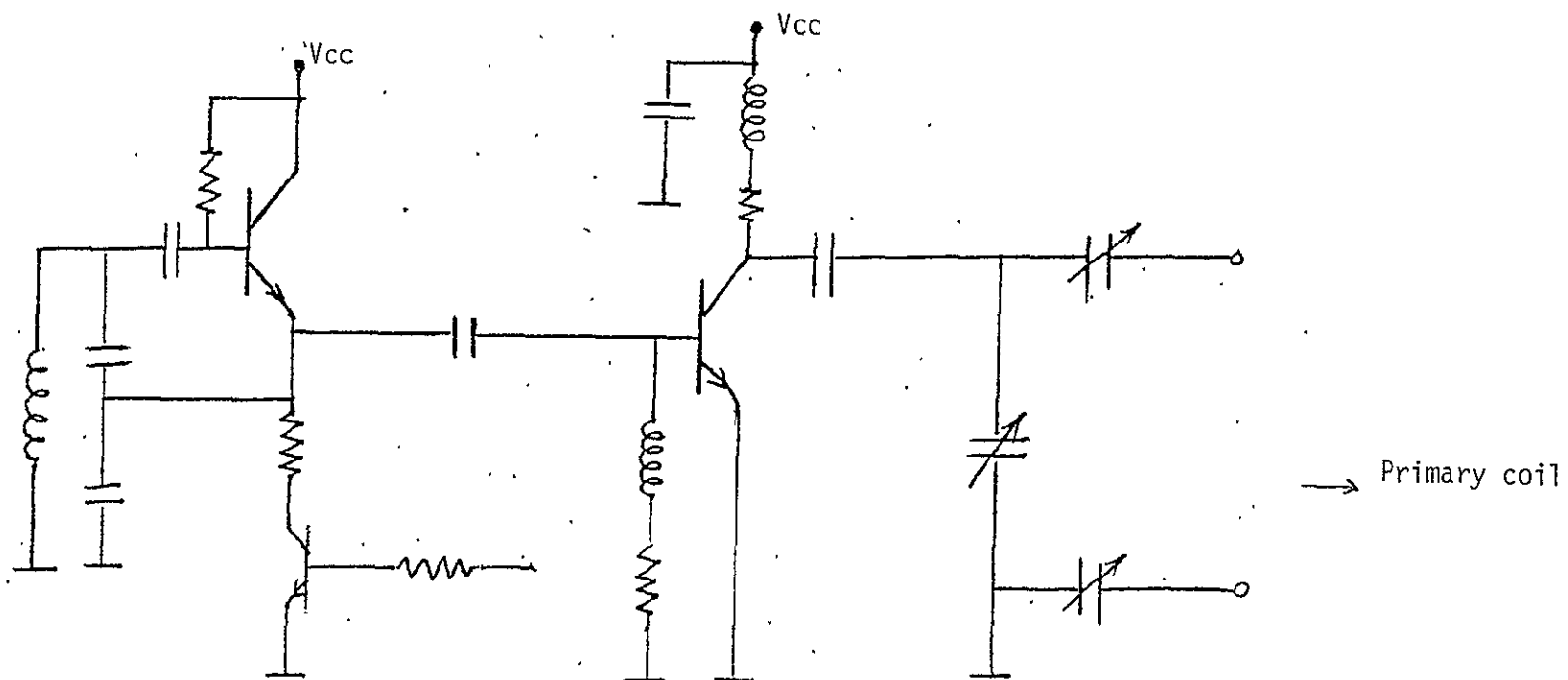
Vcc

Vcc

Primary coil

Fig. D-25   RF powering circuit

transmitting coil. Main consideration concentrates on the efficiency of the power delivery, which depends on the Q values of the coils and the distance between the two coils. The RF powering unit basically consists of an RF oscillator followed by a power amplifier matched into the tuned primary tank. The circuit is shown in Fig.D-25.

System Performance

	Power Supply (Vcc)	Supply Current	Clock rate
Implant Unit	7 volt	250 μA	800 Hz or 200/channel
External Unit	±7.5 volt	45 mA	800 Hz

Two approaches were used to evaluate the system's performance. The first was mainly aimed at the electronic circuits. Instead of using the transduced voltage, signal from the function generator is directly fed into the modulator input and monitors the system's output with a sinusoidal wave. Frequency response is of main interest here. Fig.D-26 shows the output recording of two arbitrary channels of the three available channels. The performance of the system can be summarized as follows:

1. 60 cycle noise:

This is mainly due to the power supply ripple of the demodulation circuit. The decoupling circuit had been used for each circuit board. The 60 cycle noise seen at the output is less than 5 mV.

2. Cross talk:

With an input of a 5 volt peak-to-peak sinusoidal wave, the cross talk measured is about -60dB, which is also the typical CMOS multiplexor value.

3. Line coupling noise:

The output of the scope appears as spikes, the amplitude is about 15 - 20 mV. Since it is measured after the 120 Hz High-cutoff low pass RC filter, probe pick-up is of high possibility.

4. · Sensitivity:

Sensitivity is defined here as $\frac{\Delta V \text{ out}}{\Delta V \text{ in}}$. It is dependent on the degree of pulse-position modulation and also the slope of the sampling ramp. With the present setting the sensitivity is about 0.75.

5. Frequency response:

Different input frequencies were applied and the system output was recorded. (The sampling rate of the data was set at 300/sec when taking this data). Since the information content is well within 100 Hz, any frequency higher than this was not tested. The attenuation of the higher frequency shown in Fig. D-26, is mainly due to the frequency response roll-down of the chart recorder.

6.. ·Sampling, holding drift:

The holding capacitor is 4700 pF. The only discharging pathways are through the buffer amplifier input and the analog gate. Both of these have a resistance value of greater than 10^{10} ohms. RC constant in any event should be larger than 20 seconds. The drift seen at the output is less than 4 mV.

7. The pulse position linearity is shown in Fig. D-27. It shows that the conversion factor is 16 mV for 1 μsec pulse position change.

The second approach to test the system has the sense of completion since it includes the transducer stage. The entire implant unit is placed into the oven for controlled temperature testing. The pressure transducer was kept in a well-sealed test tube with a variable pressure arrangement. The EKG channel is grounded. The data monitored at output is plotted in Fig. D-28. Sensitivities measured are 10.9 mV/mmHg and 20 mV/.1°C for the pressure and temperature channels respectively. The temperature coefficient of the pressure channel is about 22 mV/.1°C. A good shielding of the implant unit is necessary to avoid the influence due to the strong RF powering field. Fig. D-29 shows the difference seen at pulses received by demodulation unit before and after the shielding. The present discrete circuit form may be the reason for the gittering noise experienced, which limits the resolution to about ±1mmHg and ±.1°C. It is quite certain that after fabrication of the hybrid circuit, this gittering noise will be improved.

Temperature compensation for pressure channel

The temperature coefficient of the pressure transducer is negative for our bridge, i.e. the higher the temperature, the lower the pressure reading for an unchanged pressure. The compensation circuit will add a suitable amount of voltage to the

60 Hz   I   80 Hz   I   100 Hz   I

0.2 Hz   I   2 hz   I   20 Hz   I   40 Hz
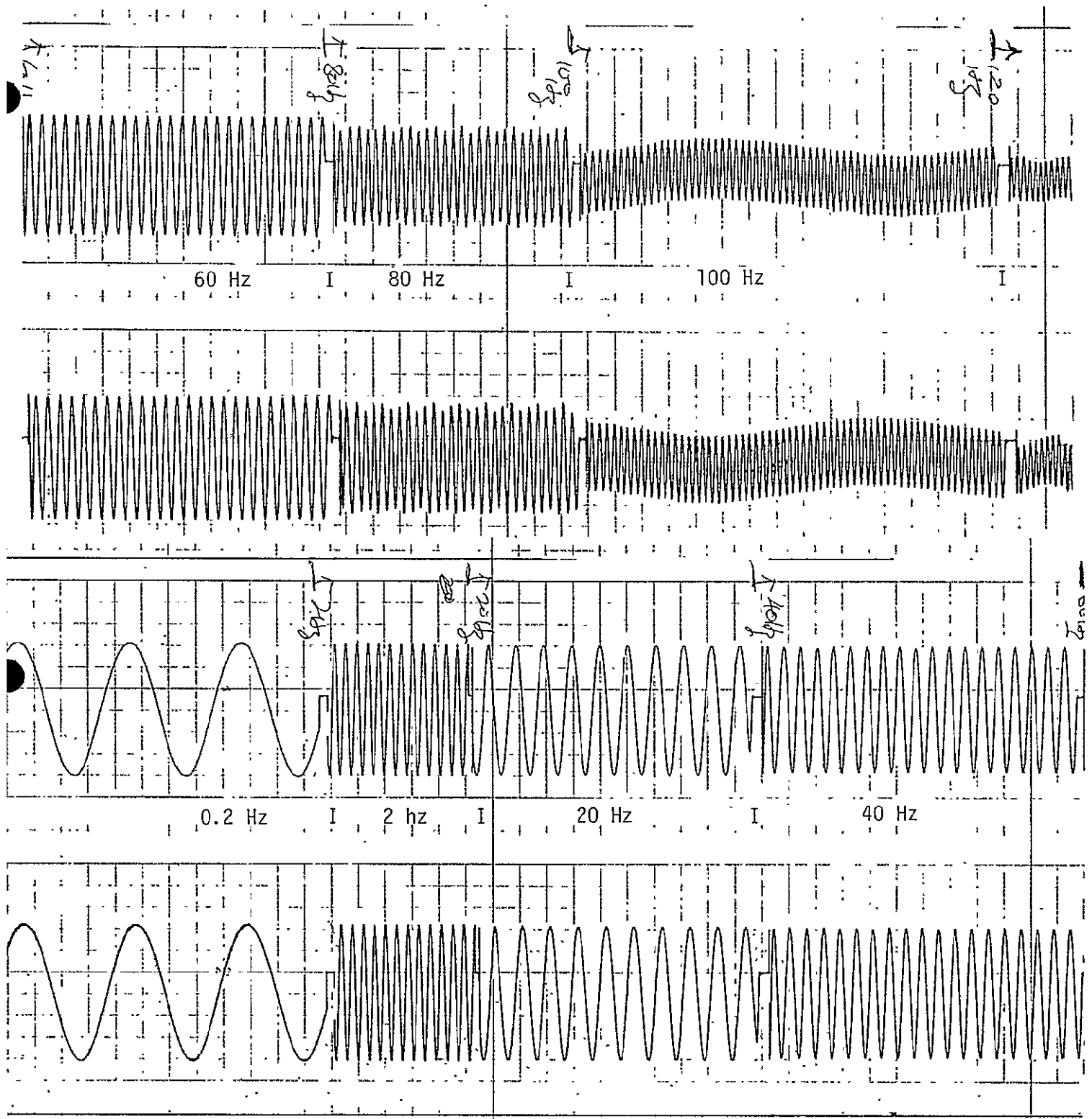
A-40

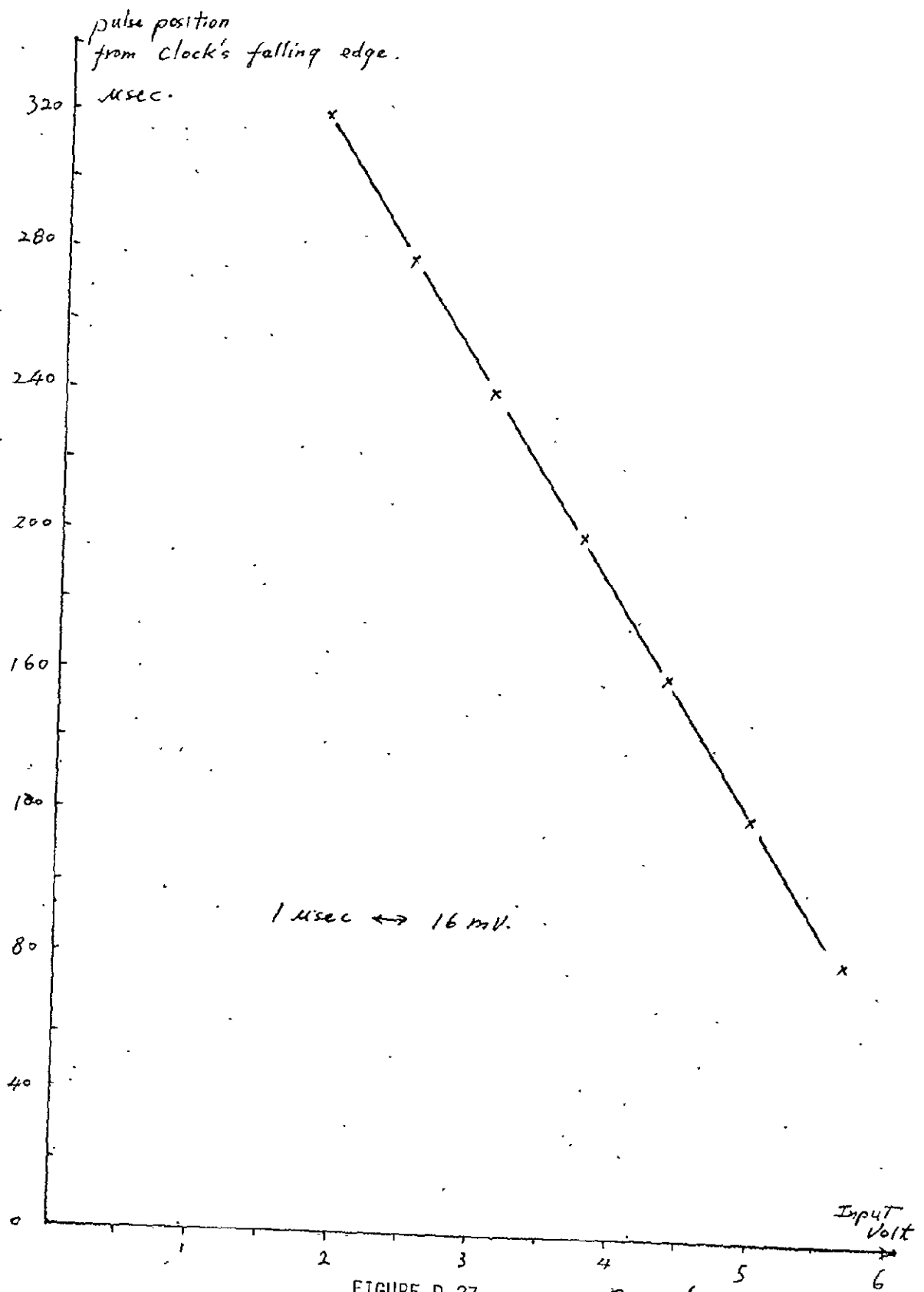Fig. D-26   Frequency test.   Recording of arbitrary
two channels.

FIGURE D-27

A-41
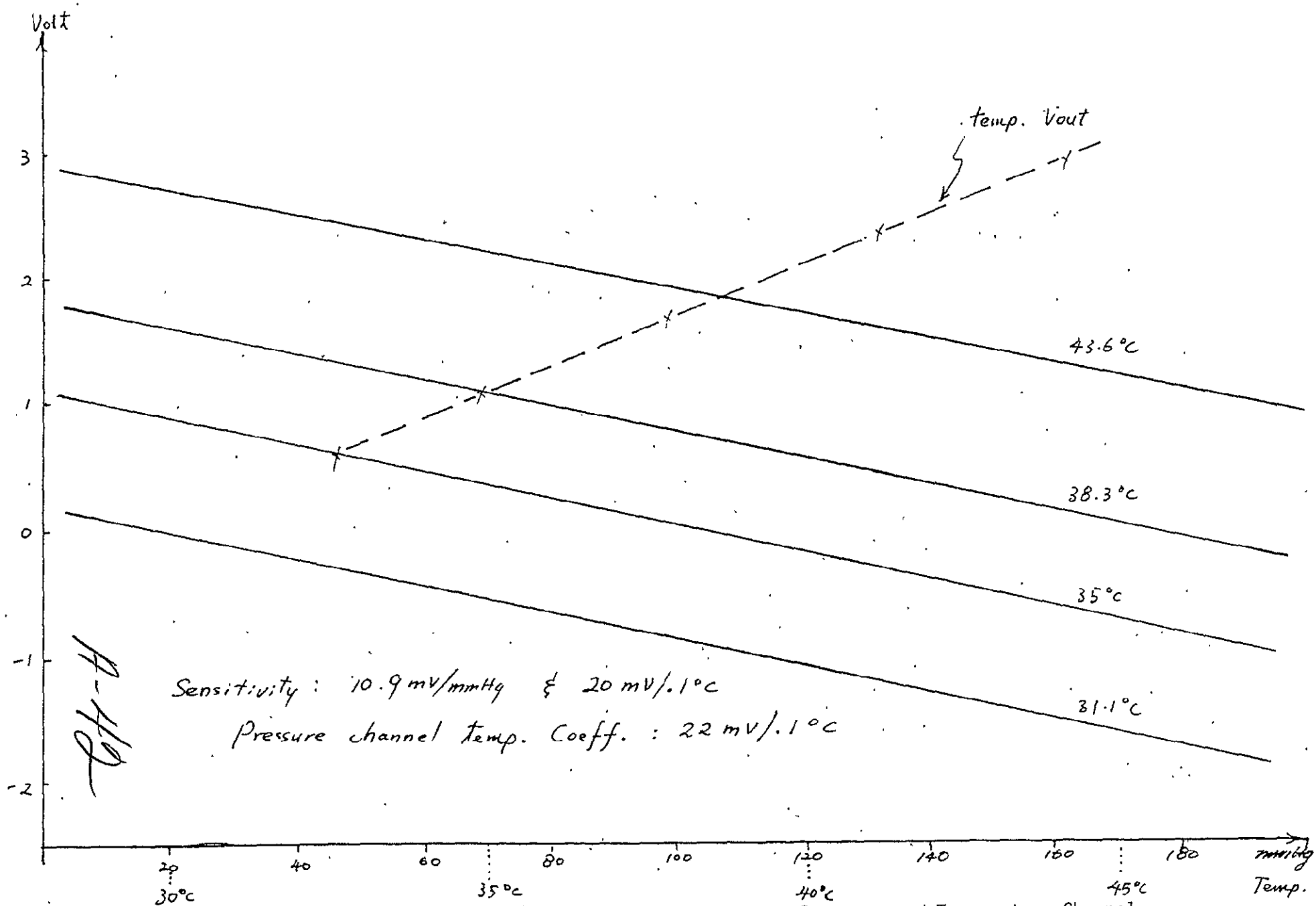
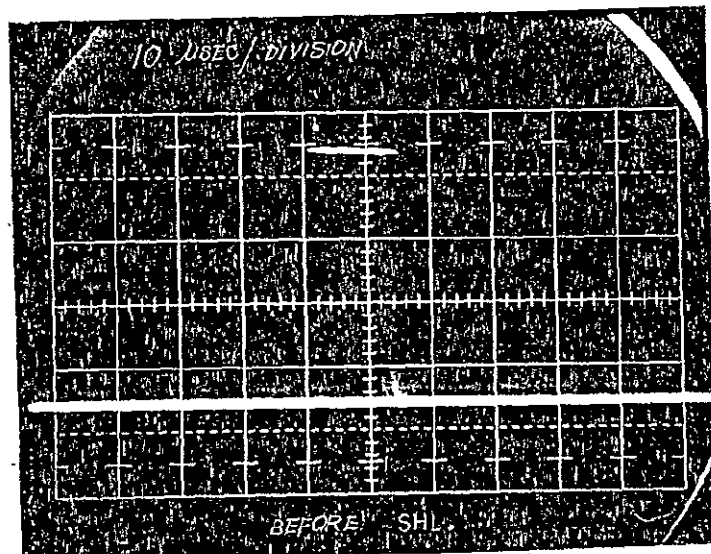FIGURE D-28 System Performance of Pressure and Temperature Channel

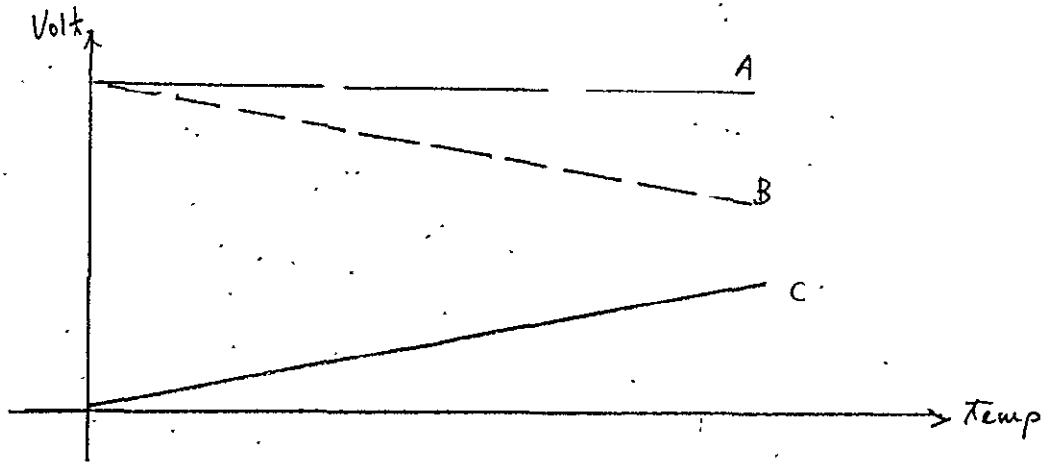Sensitivity : 10.9 mV/mmHg & 20 mV/.1°C

Pressure channel temp. Coeff. : 22 mV/.1°C
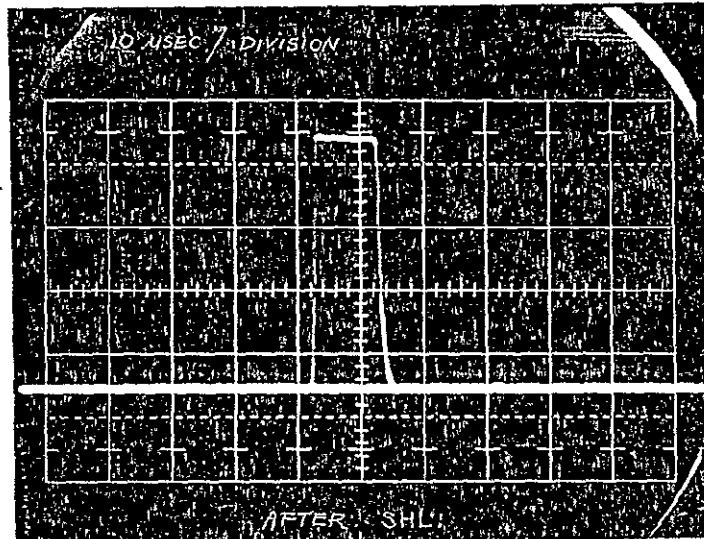
After the shielding

Before the shielding

Fig. D-29 Shielding effect of the transducer amplifier

A-43

pressure channel output and hence cancel the temperature influence. The idea is shown in the following figure:

Curve B represents the uncompensated output voltage against temperature range. The compensating curve, curve C, has a slope of the same absolute value as of curve B but opposite in sign. The resultant curve A will then represent a constant pressure over the temperature variation. The offset of curve A will depend on that of curve B and will be adjusted at calibration.

Figure D-30 shows the relation of the temperature channel output and the pressure channel temperature variation for a constant pressure source. Both are linearly approximated.

The circuit then consists of a first Op. Amp. to obtain the curve C from the temperature channel output and a second Op. Amp. to add this curve C to the pressure channel output. The circuit is as shown in Fig. D-31.

Pressure transducer packaging

The semiconductor pressure transducer fabricated in MEL has the dimensions of 150 x 50 x 10 mils. Various catheter-tip mounting, utilizing the advantage of the small size of the sensor, have been tried and each shows a common problem due to the reaction of body fluid leakage which made contact with the sensor. The proposed packaging is shown in Fig. D-32. The basic objective is to separate the transducer from the body fluid by a second fluid which is non-conductive. As can be seen from the drawing in Fig. D-32, the package consists of a diaphram made with latax and two stainless steel parts - part A and part B. Half of the wall of part B is cut to provide a larger area for pressure transmitting while still providing mechanical protection to the sensor. A latax diaphram encircles whole of part B and
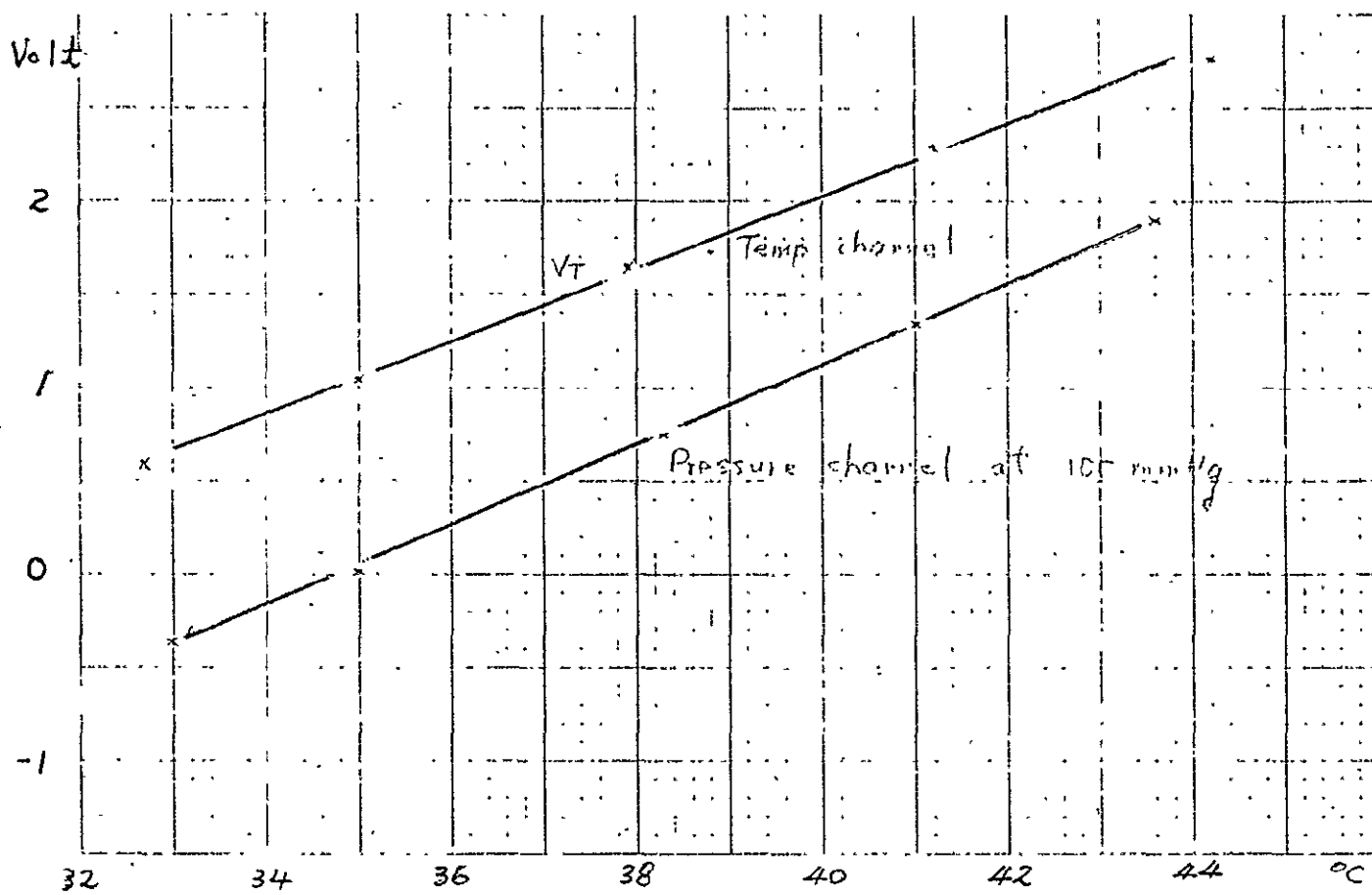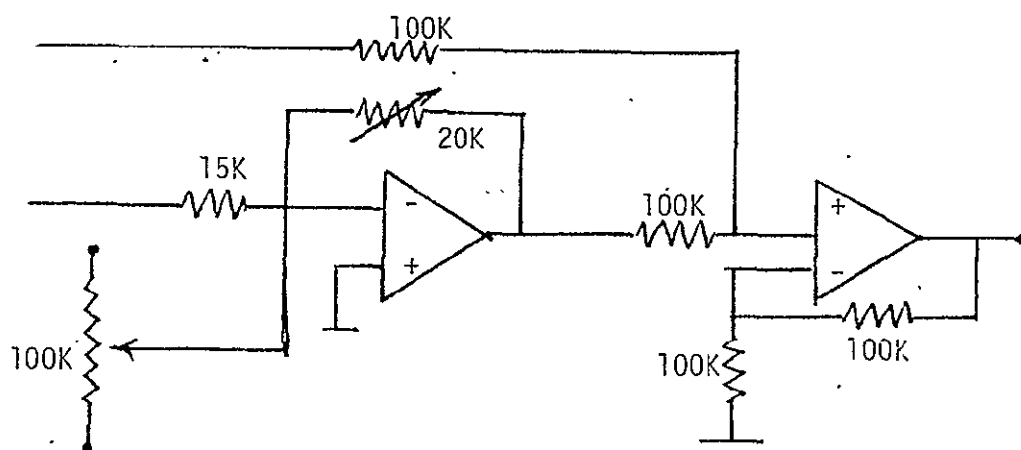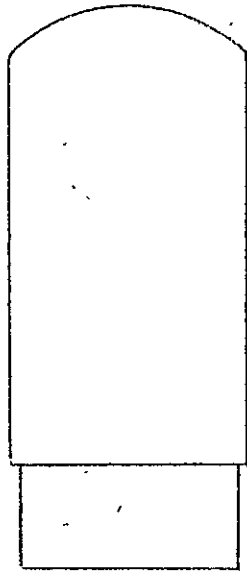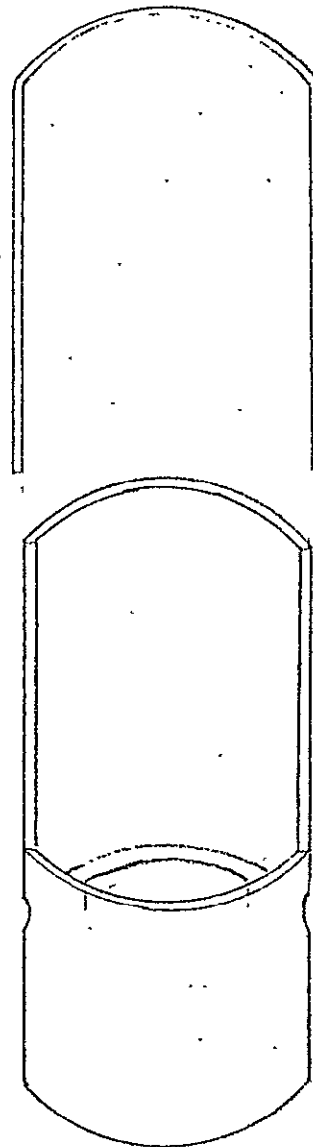
A-44

Fig. D-30

Fig. D-31   Compensating circuit

A-45

Latax Diaphram....

Part B.....

Pressure transducer

Finishing outlook
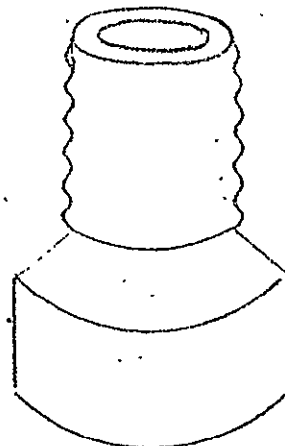
Part A..

Fig. D-32 Pressure transducer
packaging assembly

is bonded to its base. Sensor leads run through the center hole of part A. The hole is then sealed with RTV. The sensor rests on top of part A with a distance of about 2 mm. Sensor leads also serve as the supporting structure. The inside space is filled with silicon grease, which is the above mentioned "second fluid". The sealing process will be done in the silicon grease in the vacuum to insure that no air bubbles will be trapped inside the package.

The entire unit at present has a diameter of 160 mils and is 500 mils in length. However, it is only the first unit under test and it is believed that further size reduction can be obtained after successful development of the entire procedure.

RF POWERING WITH RECTANGULAR CAGE

Introduction

The rectangular cage is originated from the cylindrical cage. The distribution of the magnetic field, as shown below, in the two cages are similar to each other. At present, an RF powering system with a rectangular cage is built and some measurements have been made. The first section of this report describes the design of the cage and of the entire RF powering system.

End View
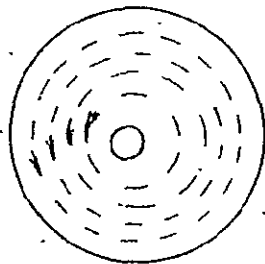
Cylindrical Cage
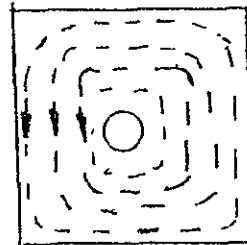
Rectangular Cage

The direction of the magnetic field inside the cage surrounds the central rod. Therefore, a three-dimensional detector is required to pick-up the RF power, independent of the direction of the detector. The three-dimensional detector is discussed in the second section.

The leakage power of the cage is also an important item. It must be below a certain limit in order not to interfere with other instruments in the neighborhood of the cage. The measurement of the leakage power of the cage is given in the third section.

When the animal is placed in the cage, the eddy current on the body of the animal will cause detuning and mismatching effects. The higher the Q value of the cage, the more serious these effects will be. A suggestion to compensate these effects, due to the movement of the animal, by automatic tuning and matching is proposed in the final section.

Design of the Rectangular Cage and the RF Powering System

The configuration of the cage and the magnetic field inside the cage are shown in Figure 1. The flowing path of the current I builds up a magnetic field B which is inversely proportional to the radial distance from the central rod and is independent of the axial position. B is given by:

$$B = \frac{\mu_o I}{2\pi r}$$

where r is the radial distance from the central rod.

If r is very small, B will be too high and so will the DC pick-up voltage (above five times the minimum value required). Then the regulator following the detector will not be able to regulate the detected voltage within the limited range. Therefore, the central rod is surrounded by a plastic tube so that the animal cannot reach this region.

The slots on the two sides of the cage are parallel to the flowing path of the current in order that the current and the field inside of the cage will not be disturbed.

The rectangular cage can be considered as an end-shorted coaxial cable. As the length of the cage is much shorter than the wavelength, the cage is a high Q inductor. The equivalent inductance is given by:

$$L = \frac{\mu_o 1}{2\pi} \left(\ln \frac{b}{a} \right)$$

where 1 is the length of the cage (in meters)

b is the equivalent outer diameter of the cage

a is the diameter of the central rod.

In this case, 1=40 inches=1m;

$$b = \frac{20(1 + \sqrt{2})}{2} = 24 \text{ inches}$$

a = 1 inch

A-49

hence, L=0.64μh. While the system is operating.at 30 MHz the tuning capacitance
is 44 pF.

The block diagram of the RF powering system is shown in Figure 2. The 30 MHz
signal is switched by 1 KHz pulses before being sent to the power amplifier. The
pulsed RF signal supplies power to the cage, at the same time it provides a clock
signal to the modulator of the implanted telemetry. A 68 KΩ resistor parallel to
the tank circuit is used to reduce the Q value of the cage slightly for system
stabilization.

Three-Dimensional Detector

The circuit configuration and diagram of the three-dimensional detector are shown
in Figure 3. Two perpendicular ferrite-core coils and an air-core coil are utilized
to pick-up the RF power. The reason for using two ferrite-core coils and an air-core
coil is to make the entire package flat. The positions of the three coils are arranged
symetrically to minimize mutual inductances.

If the three coils are serially connected, as shown below, higher pick-up DC
voltage can be obtained and the ripples due to the variation of the direction of the
detector are reduced.
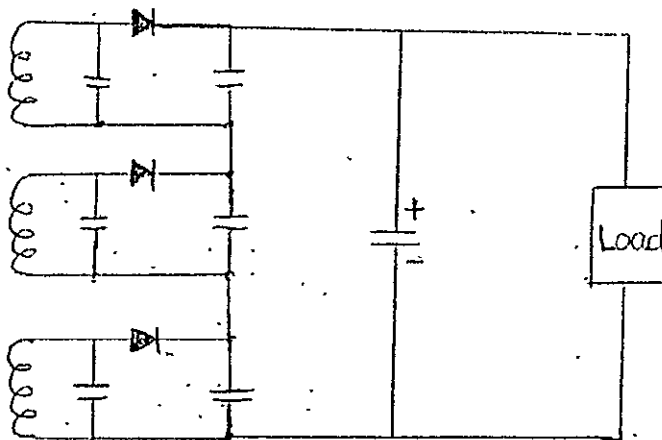
However, the air-core coils should also act as the oscillator coil of the implanted

transmitter. Therefore, serial connection of the three coils is not proper. An alternate solution is shown in Figure 3 -- two ferrite-core coils are serially connected and the air-core coil is parallel to the former two.

The performance of the detector is shown in Figure 4. The pick-up voltage decreases rapidly as tje radial distance exceeds ten inches, i.e. the detector is located in the corners of the cage. However, the possibility of the detector being located in the corners is very small. It would be satisfactory that the pick-up voltage is above the minimum voltage required at r=12 inches. A 3-4 watt input power is necessary to achieve this.

To obtain the effective permeability as high as possible, the length of the ferrite cores must be at least three times its diameter. In this case, the diameter of the core is 1/4", the length is 3/4", and the permeability of the material is about 30. Hence, the effective permeability, μ_e, is determined by:

$$\frac{\mu_e}{\mu_0} = \frac{\mu/\mu_0}{1 + 0.1(\mu/\mu_0 - 1)} = 7.7$$

Therefore, the area of the air-core coil is designed to be about eight times the cut area of the ferrite-core. Then the three coils will pick-up equal DC voltage.

The three coils are specified as below:.

Coil 1 and 2:   Core: Diameter 1/4".

                         Length   3/4"

                         permeability = 30 at 30 MHz

             Wire: #28

        No. of turn: 7-3/4

Coil 3:   Size: 1/2"x7/8"x1/8"

             Wire: #24

      No. of turn: 7-3/4

The loaded Q of the three tank circuits is about 25.

Leakage Power of the Cage

The test circuit shown in Figure 5 is set-up to measure the field strength out of the cage, which is the difference between the two field strengths measured as the cage is the load of the power amplifier and as a shielded 50 ohm resistor is the load. The point of this test circuit is that the leakages of the signal generator, power amplifier, and power meter are cancelled by taking the difference between the two measurements. Therefore, the pure leakage of the cage can be obtained.

However, the measured result is an approximate value, because the measurements are made under the assumption that the two fields for different loads of the power amplifier are in phase. Of the requirement of accuracy is not high, this method of measurement is convenient and satisfactory. The result is shown in Figure 6.

Automatic Tuning and Matching

The detuning and mismatching effects due to the movement of the animal depend on the Q value of the cage, the size of the animal, and the position of the animal (the closer to the power-in end of the cage and the central rod, the longer these effects will be).

For compensation of these effects, an automatic tuning and matching circuit is shown in Figure 7. The tank circuit is tuned at the frequency which is slightly lower than the input frequency (30 MHz in this case). The reflection signal of the power meter is taken as the error signal. It is amplified to vary the capacitances of the varactors. Finally, the tuning circuit will resonate at the input frequency and the reflection power will be zero.
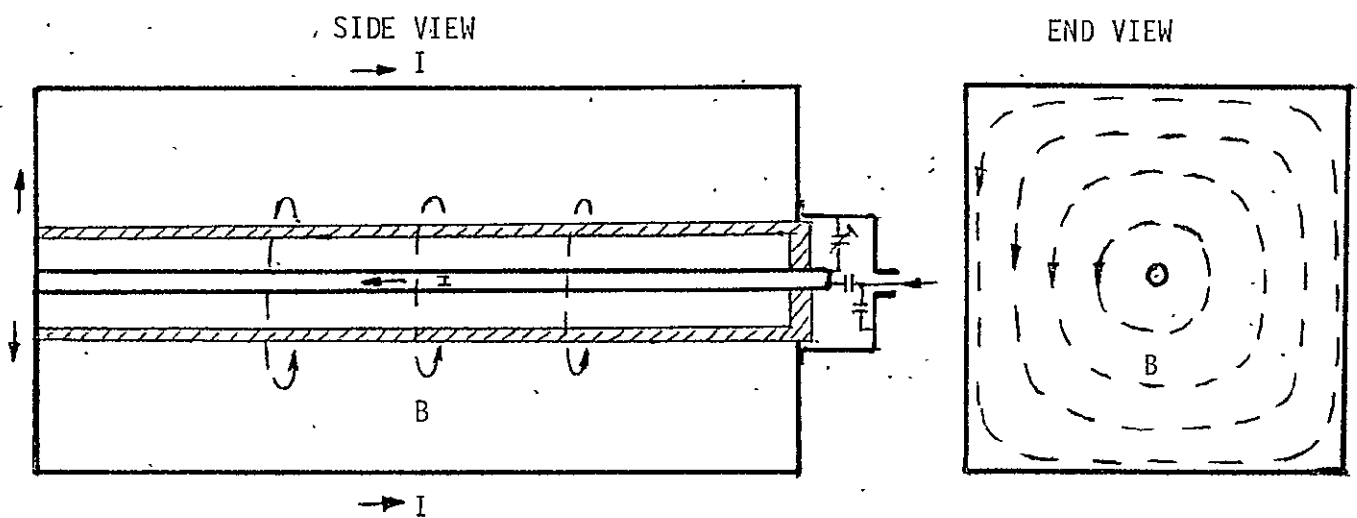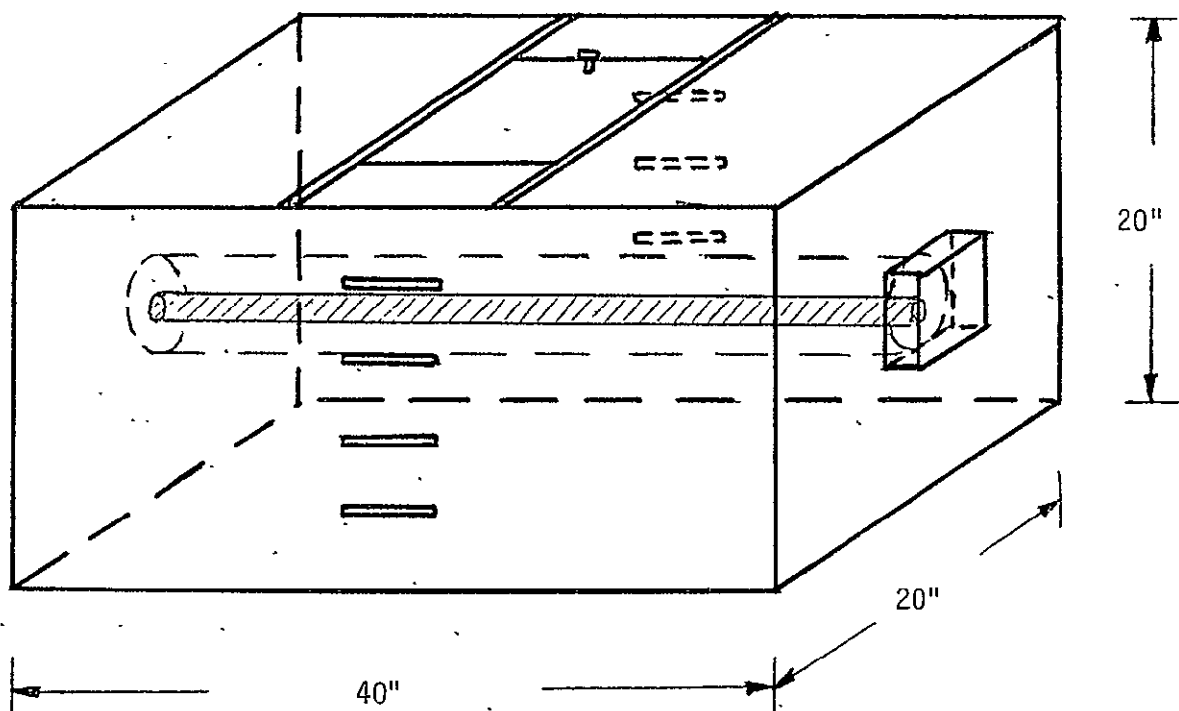
20"

20"

40"

SIDE VIEW

→ I

B

→ I

END VIEW

B

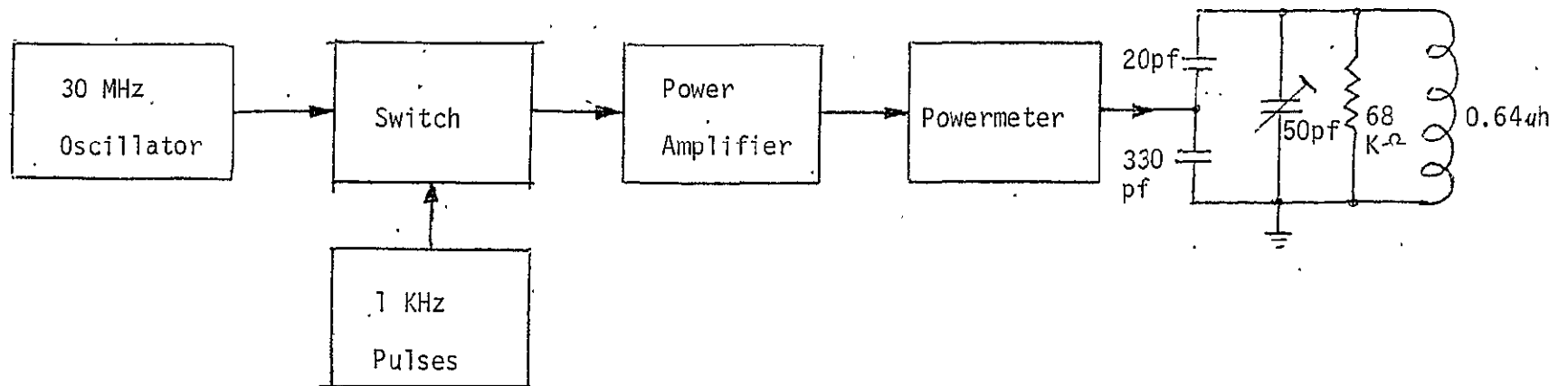Figure 1   THE CONFIGURATION OF THE CAGE

Figure 2   BLOCK DIAGRAM OF THE RF POWERING SYSTEM
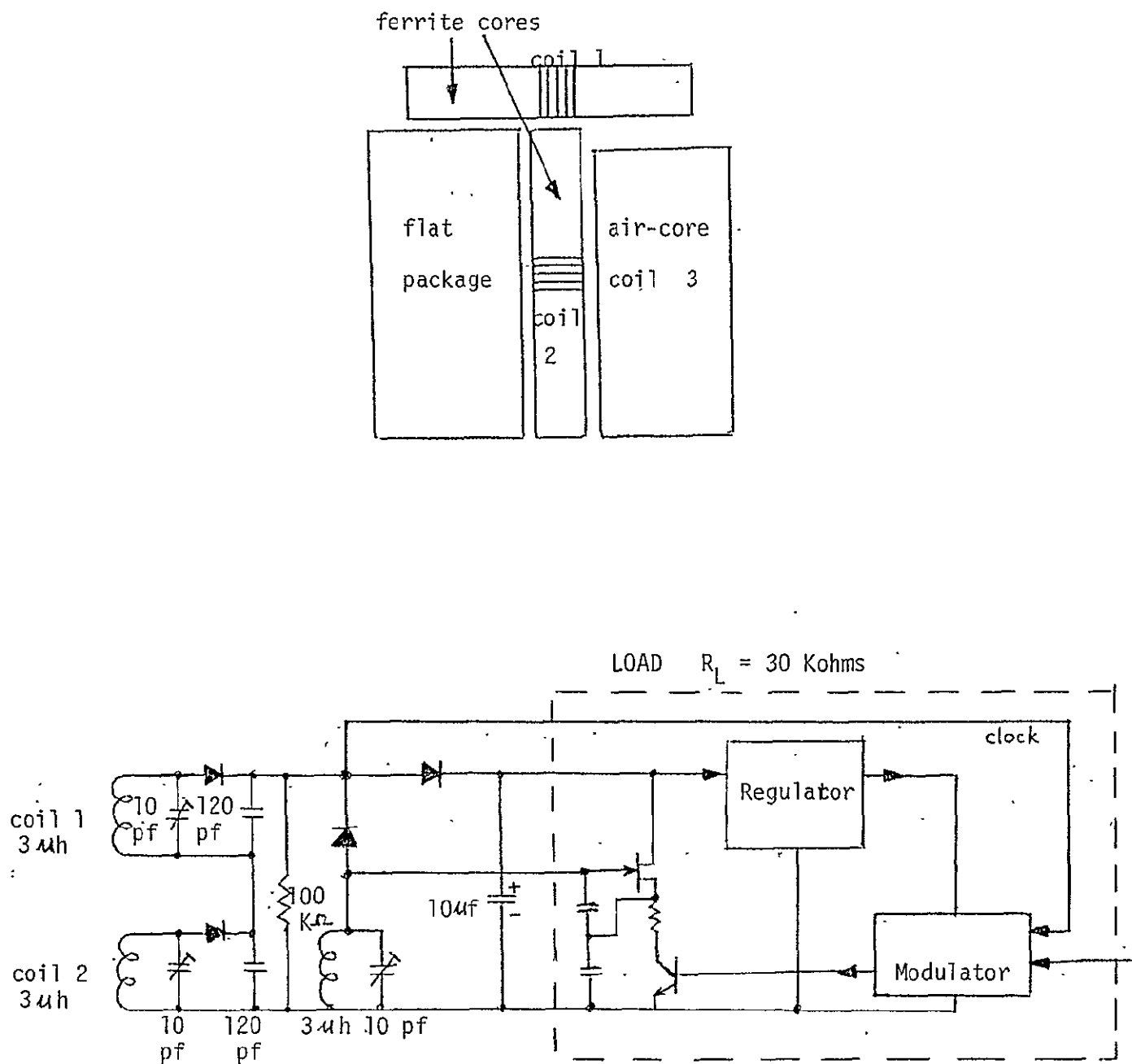
Figure 3   THE CONFIGURATION AND CIRCUIT DIAGRAM OF THE THREE-
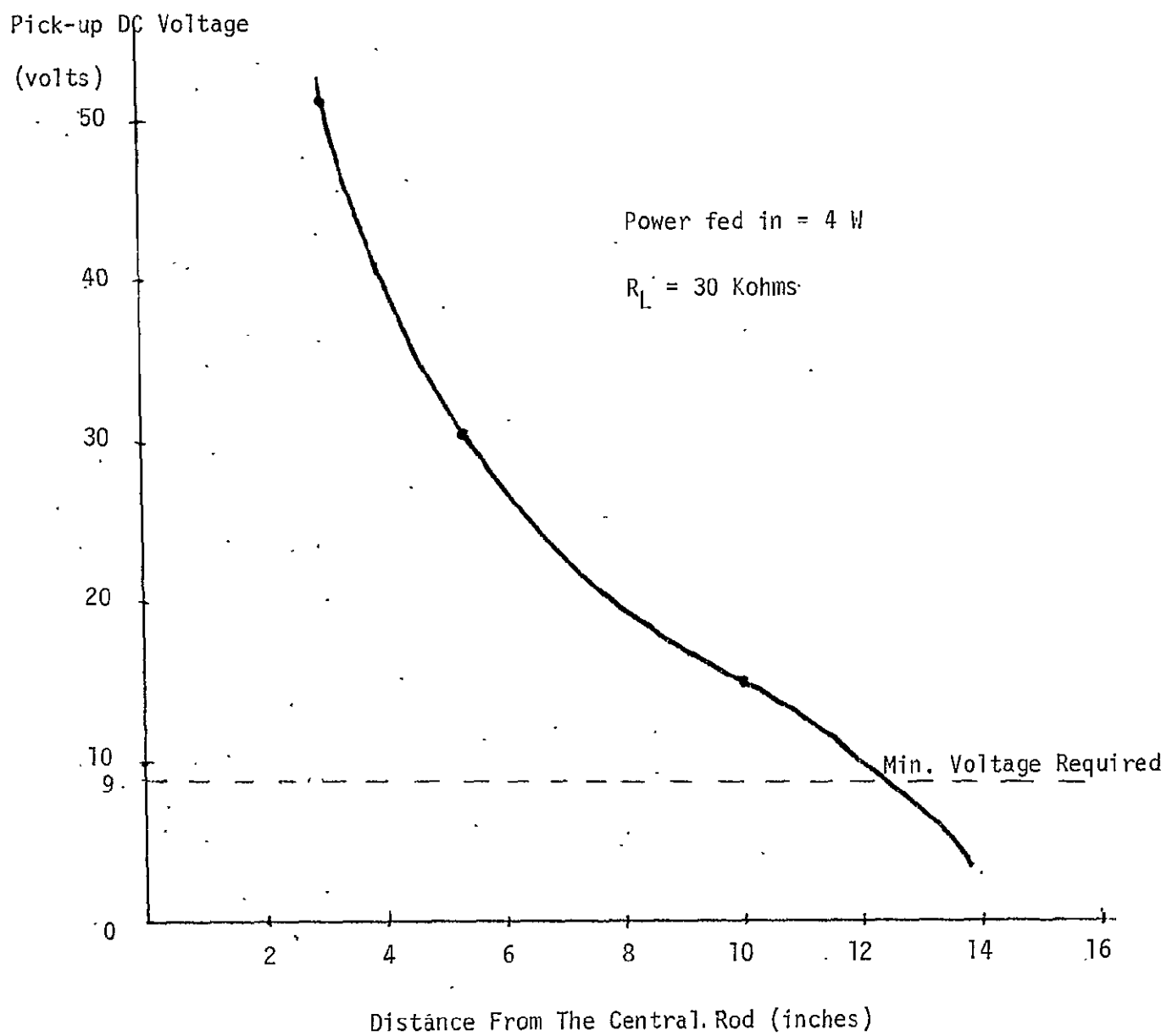DIMENSIONAL DETECTOR

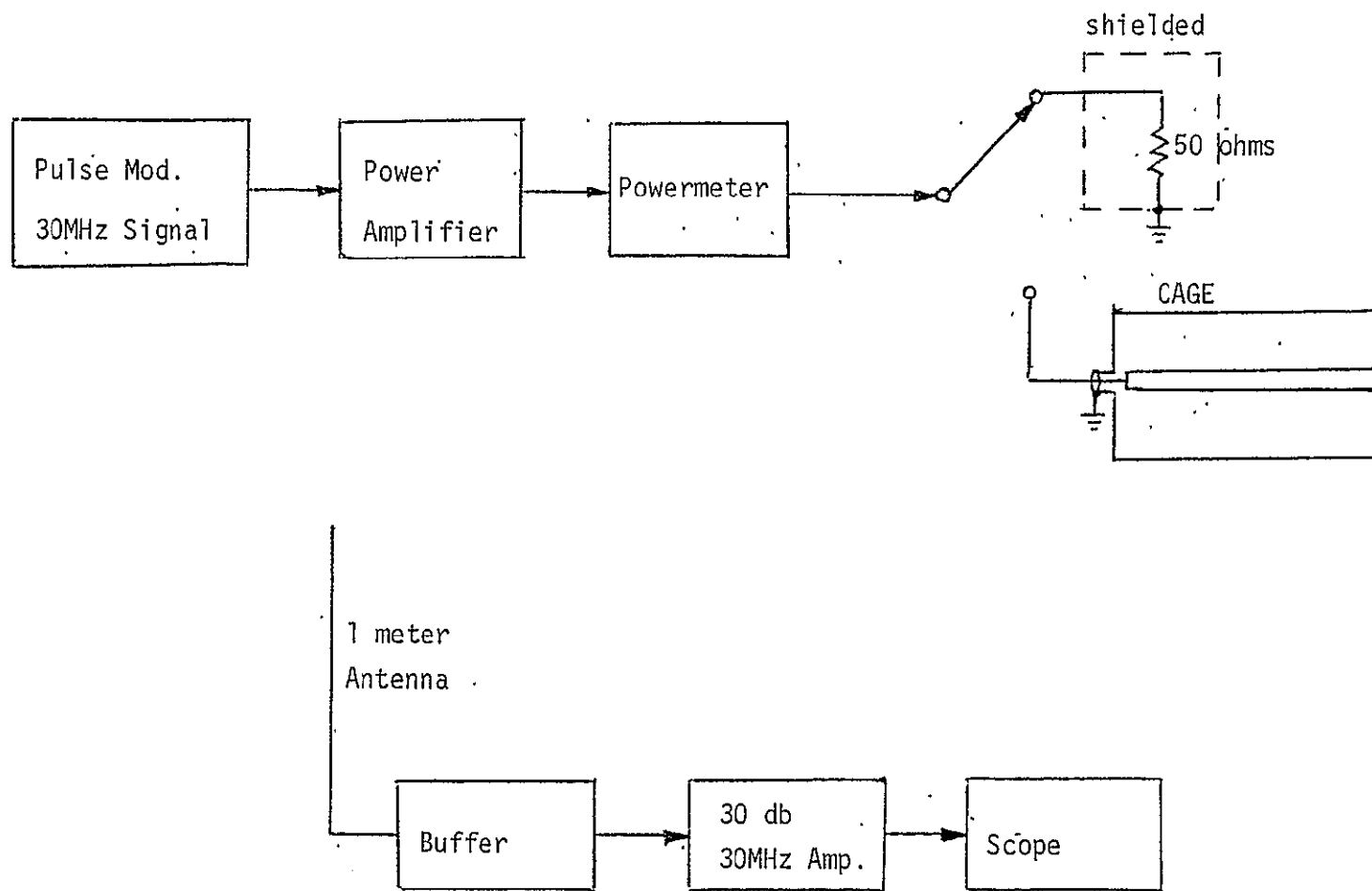Figure 4 · PICK-UP DC VOLTAGE OF THE DETECTOR
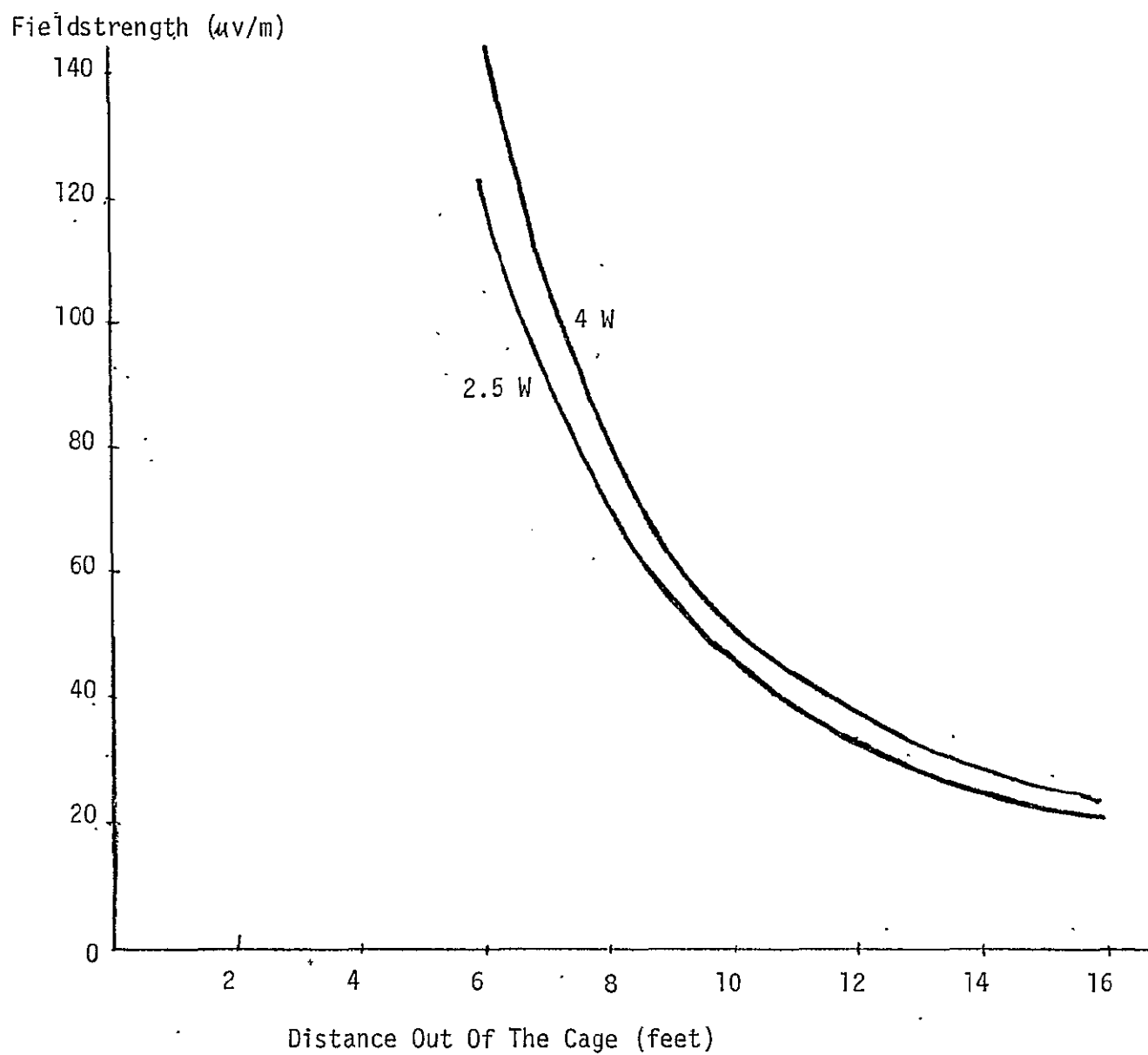
Figure 5   MEASUREMENT OF THE LEAKAGE OF THE CAGE

Figure 6   FIELDSTRENGTH OUT OF THE CAGE

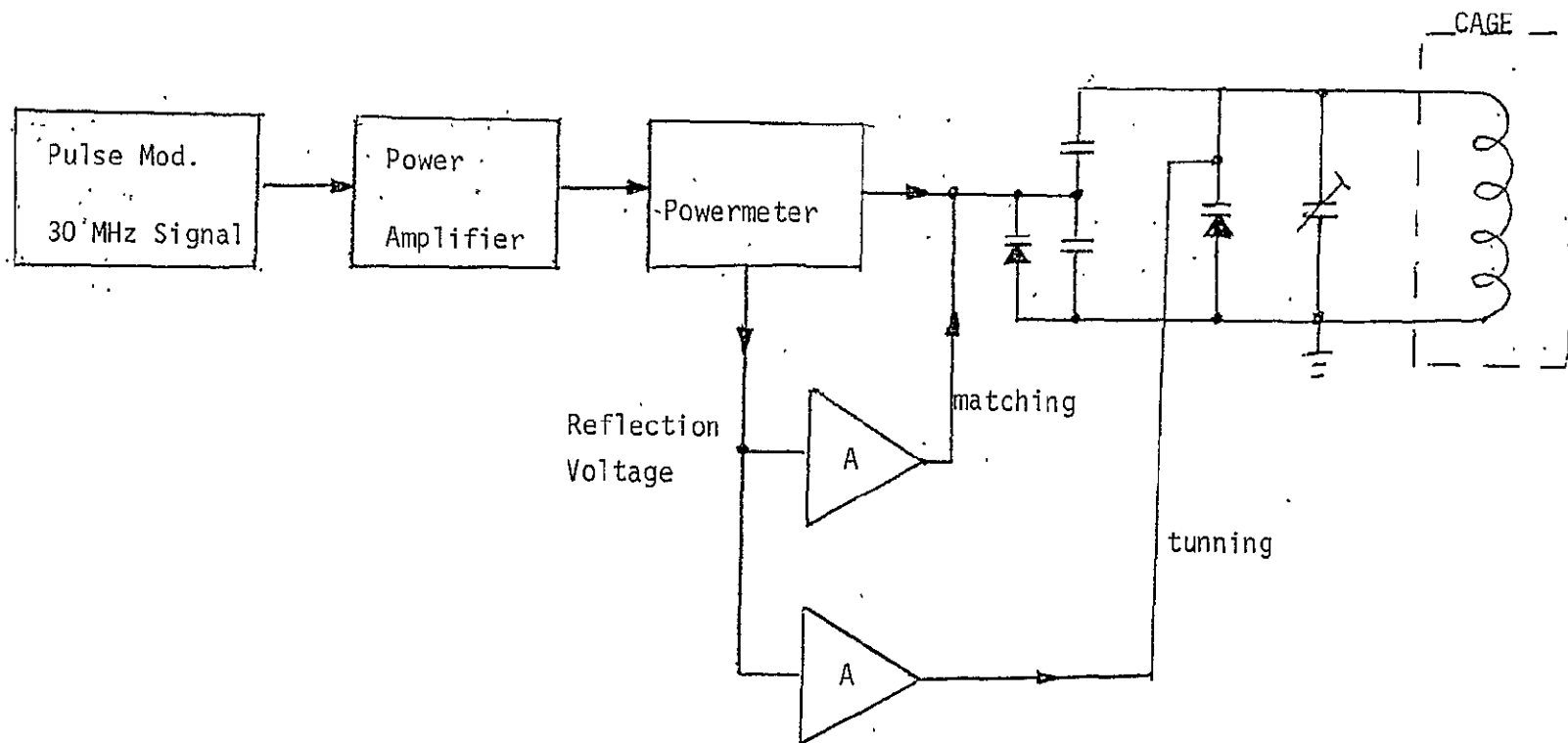CAGE

Pulse Mod.

30 MHz Signal

Power

Amplifier

Powermeter

Reflection

Voltage

matching

A

A

tunning

Figure 7   AUTOMATIC TUNNING AND MATCHING

SINGLE FREQUENCY RF POWERING

Introduction:

The single channel RF powered ECG transmitter described in pages 5-11 of the 1974-1975 progress report was packaged and implanted in a monkey at the Marine Biomedical Institute in Galveston. The initial units were not hermetically sealed and failed a few months after implantation. A hermetically sealed package was developed to prohibit any leakage of body fluids into the implant. The package is a capsule which incorporates a glass to kovar seal. A transistor header is soldered to the kovar section to complete the hermetic seal. The package is illustrated in Figure 1.
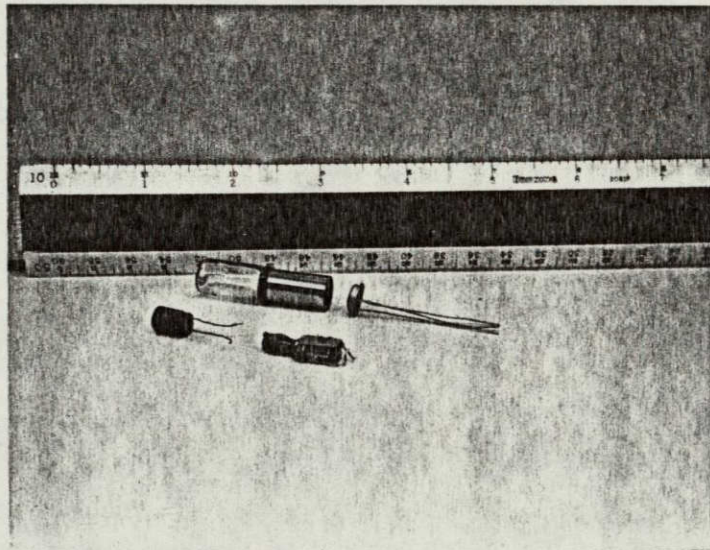

Figure 1 Components for Hermetically Sealed Package

Based on measurements taken with the hermetically sealed units, circuit modifications have been made. The external components have remained essentially unchanged; however, the implant circuitry has been modified to improve its performance. A description of the modifications to the implant will be presented in the following paragraphs.

Implant Modifications:

Test results on the implanted transmitter showed that the unit lacked sufficient transmission range and that the RF powering was marginal, necessitating very close proximity between the implant and the powering coil. Several modifications were made to the implant circuit to counteract these problems. They will be discussed on a section by section basis.

The modified oscillator is shown in Figure 2. Two significant changes have been made. First, the inductor L which in the hermetically sealed transmitter was an air core design has been changed to a ferrite core coil. This has greatly improved the powering range. The oscillator design has been modified slightly by changing the capacitance ratio. This has changed the oscillator output as detected across C1 from approximately 300 mV DC to 5 V DC. This has significantly increased the transmission range.
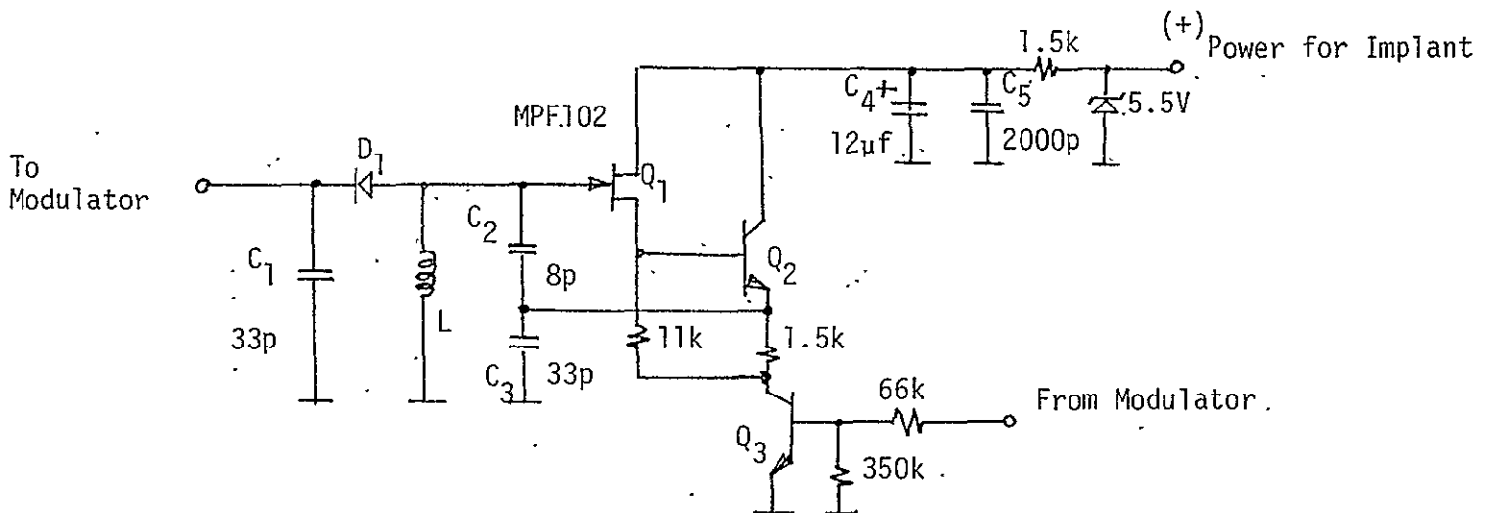
Figure 2 . Oscillator

The higher oscillator output presented a problem in the modulator in that it caused the transmitter to retrigger itself. The modulator, therefore, was modified to eliminate this problem. The new modulator circuit is shown in Figure 3. Transistor Q_7 has been added to inhibit triggering the modulator with the transmit pulse from the oscillator.
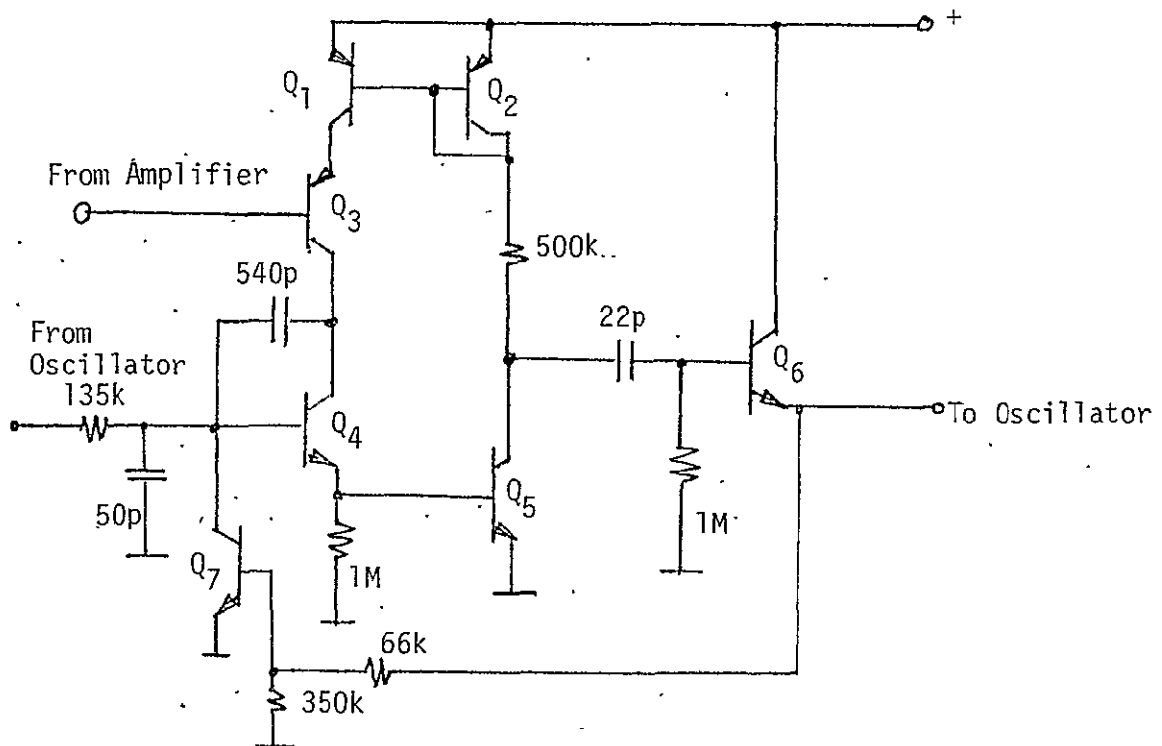

Figure 3   - Modulator

The increased RF level caused saturation problems with the input amplifier. The circuit diagram is illustrated in Figure 4. The design was changed to eliminate the diodes in series with the amplifier inputs. These diodes were necessary for level shifting; however, they also tended to rectify the RF present at the input. The new design, shown in Figure 5, accomplishes the level shift through the use of a resistive network.

A new transmitter consisting of the modified circuits is under evaluation. As soon as testing is complete, it will be packaged and implanted to further study its characteristics.
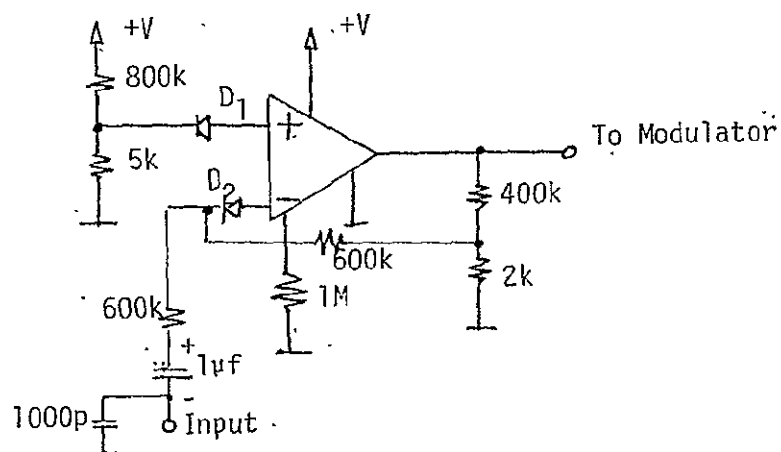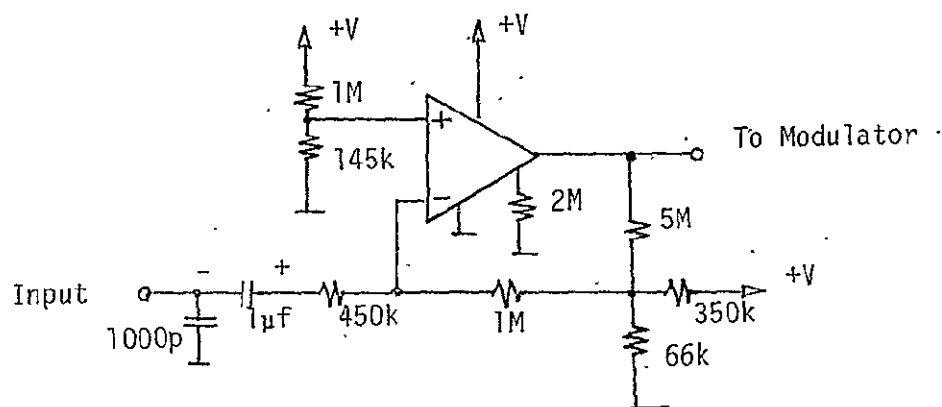

Figure 4   Original Amplifier

Figure 5   Modified Amplifier

APPENDIX B

PUBLICATIONS

PUBLICATIONS NOT PREVIOUSLY REPORTED

1. W.H. Ko, J. Hynecek, and A. Kou. "An Implantable Single Frequency RF Power-ed Telemetry System." 3rd International Symposium on Biotelemetry, May 17-20, 1976.

2. A. Kou. "A Single Frequency RF Powered Three Channel Telemetry System." M.S. Thesis, June 9, 1976.